Physical and Biogeochemical Properties of Rotten East Antarctic Summer Sea Ice

M. Corkill[1] , **S. Moreau[2]** , **J. Janssens[3]** , **A. D. Fraser[4]** , **P. Heil[4,5]** , **J.-L. Tison[6]** , **E. A. Cougnon[7]** , **C. Genovese[6]** , **N. Kimura[8]** , **K. M. Meiners[4,5,9]** , **P. Wongpan[4]** , and **D. Lannuzel[1,9]**

[1]Institute for Marine and Antarctic Studies, University of Tasmania, Hobart, TAS, Australia, [2]Norwegian Polar Institute, Tromsø, Norway, [3]Commonwealth Scientific and Industrial Research Organisation (CSIRO), Hobart, TAS, Australia, [4]Australian Antarctic Program Partnership, Institute for Marine and Antarctic Studies, University of Tasmania, Hobart, TAS, Australia, [5]Department of Climate Change, Energy, the Environment and Water, Australian Antarctic Division, Kingston, TAS, Australia, [6]Laboratoire de Glaciologie, Département Géosciences, Environnement et Société (DGES), Université Libre de Bruxelles, Bruxelles, Belgium, [7]Integrated Marine Observing System, Australian Ocean Data Network, University of Tasmania, Hobart, TAS, Australia, [8]Atmosphere and Ocean Research Institute, The University of Tokyo, Kashiwa, Japan, [9]Australian Centre for Excellence in Antarctic Science, Institute for Marine and Antarctic Studies, University of Tasmania, Hobart, TAS, Australia

Abstract Sea ice forms a barrier to the exchange of energy, gases, moisture and particles between the ocean and atmosphere around Antarctica. Ice temperature, salinity and the composition of ice crystals determine whether a particular slab of sea ice is habitable for microorganisms and permeable to exchanges between the ocean and atmosphere, allowing, for example, carbon dioxide (CO_2) from the atmosphere to be absorbed or outgassed by the ocean. Spring sea ice can have high concentrations of algae and absorb atmospheric CO_2. In the summer of 2016–2017 off East Antarctica, we found decayed and porous granular ice layers in the interior of the ice column, which showed high algal pigment concentrations. The maximum chlorophyll *a* observed in the interior of the ice column was 67.7 µg/L in a 24% porous granular ice layer between 0.8 and 0.9 m depth in 1.7 m thick ice, compared to an overall mean sea-ice chlorophyll *a* (± one standard deviation) of 13.5 ± 21.8 µg/L. We also found extensive surface melting, with instances of snow meltwater apparently percolating through the ice, as well as impermeable superimposed ice layers that had refrozen along with melt ponds on top of the ice. With future warming, the structures we describe here could occur earlier and/or become more persistent, meaning that sea ice would be more often characterized by patchy permeability and interior ice algal accumulations.

Plain Language Summary The growth and melt of Antarctic sea ice is one of the largest seasonal events on Earth. The rapid changes visible at its surface correspond to changes hidden inside the sea ice. East Antarctic sea-ice samples were collected in 2016–2017 from the icebreaker *RSV Aurora Australis* to investigate the internal structure of sea ice in summer. Capping the sea ice, impermeable layers inhibited vertical transfer of material through the ice, but ponds had also melted through these layers to allow exchange between the ocean and atmosphere. We also found high concentrations of ice algae deep inside the sea ice, which might be inaccessible to grazers but important for absorbing atmospheric carbon dioxide. With warming temperatures, the observed ice characteristics may become more common or persist longer in each summer with potential consequences for ecosystem processes.

1. Introduction

Antarctic sea-ice growth and decay is one of the largest seasonal events on Earth with the sea-ice extent changing from ∼19 million km² in early spring to ∼3 million km² at the end of summer (Meier et al., 2021). When seawater freezes to form sea ice, salt is rejected in brine. A network of pockets and channels of residual brine inside sea ice provides a habitat for microorganisms and can make sea ice permeable to gases, solutes and particles (Light et al., 2003), allowing exchange of matter across ocean/ice/atmosphere interfaces (Meiners & Michel, 2017; Vancoppenolle, Meiners, et al., 2013). Absorbed solar radiation can melt the snow and ice at the top of the sea ice (Perovich et al., 1998). This melt can refreeze on top of or into the colder, saltier sea ice below, closing the sea-ice pores, limiting ocean-atmosphere exchange (Nomura et al., 2010; Polashenski et al., 2012; Tison et al., 2008).

Methodology: M. Corkill, S. Moreau, J. Janssens, A. D. Fraser, P. Heil, J.-L. Tison, E. A. Cougnon, C. Genovese, D. Lannuzel

Project Administration: M. Corkill, D. Lannuzel

Supervision: K. M. Meiners, P. Wongpan, D. Lannuzel

Visualization: M. Corkill

Writing – original draft: M. Corkill

Writing – review & editing: M. Corkill, S. Moreau, J. Janssens, A. D. Fraser, P. Heil, J.-L. Tison, E. A. Cougnon, C. Genovese, N. Kimura, K. M. Meiners, P. Wongpan, D. Lannuzel

Sea ice that survives into summer, when incoming solar radiation is high, can transition between permeable and impermeable states.

Brine in sea ice has a phase relationship that depends on temperature (Assur, 1958; Dieckmann & Hellmer, 2010; Feltham et al., 2006; Vancoppenolle, Notz, et al., 2013; Wells et al., 2019). Studies carried out in both hemispheres, ranging in duration from weeks to months, have described developmental stages of the internal structure of sea ice (e.g., Fritsen et al., 1994; Kawamura et al., 2004; Tison et al., 2008; Zhou et al., 2013). In winter, most of the salt from seawater is rejected from the skeletal layer (vertical ice plates that are loosely connected and constitute the bottom few centimeters) as the ice consolidates and advances downward, while remnant brine is trapped inside inclusions. When sea ice warms during spring, relatively-high-salinity brine inclusions melt sea ice to maintain thermodynamic equilibrium, thereby increasing the porosity (Petrich & Eicken, 2010). When brine inclusions connect to the underlying seawater, brine can sink out and be replaced by fresher and lighter seawater in a process called brine convection (e.g., Worster & Rees Jones, 2015) which can occur across the full depth of sea ice (Jardon et al., 2013). Brine convection can also be reinitiated by snow ice formation (Fritsen et al., 1994; Lytle & Ackley, 1996). Brine convection rapidly desalinates sea ice and the incoming seawater can replenish nutrients (Tison et al., 2008). However, strong brine convection may also detach and drain algae from the sea ice in concert with melting of brine channel walls (e.g., Galindo et al., 2014; Tison et al., 2008; Zhou et al., 2013), but this process is complex and can be disconnected from draining other organic matter (Juhl et al., 2011).

Substantial snow loads relative to ice thickness, such as those deposited in autumn in the Southern Ocean (Krinner et al., 2007), can force the top of sea ice below sea level (negative freeboard) causing flooding by seawater which seeds surface (top ice) and internal algal assemblages (Fritsen et al., 1994; Lytle & Ackley, 1996; Tison et al., 2017). If the resultant snow and seawater slush freezes to form snow ice, brine is rejected to percolate through the underlying sea ice. On the other hand, snowmelt can percolate through the snowpack and refreeze on top of or within colder and saltier sea ice below. This refrozen snow is called superimposed or interposed ice (superimposed inside pores of sea ice) and commonly seals the top of the sea ice in summer (Polashenski et al., 2012). However, the seal can be broken by brine tubes, fed by brine rejecting processes such as snow ice formation, growing down through the impermeable layers (Kawamura et al., 2004; Tison et al., 2017). Snowmelt may also drain into the brine channels, diluting them and stratifying the brine. Brine stratification limits the transport of solutes through the ice to molecular diffusion, which is a much slower process than convection that reduces nutrient availability for ice algae growth (Vancoppenolle et al., 2010). Figure 1 shows a conceptual model of the thermodynamic evolution of the internal structure of sea ice based on the processes described here and above (Table S1 in Supporting Information S1).

In addition to brine convection and surface flooding, there are several other processes that inject seawater to sea ice and help to sustain high biomasses of sea-ice algae. Snow ice layers near the top of sea ice can decay to form high-porosity gap layers, which allow lateral infiltration of seawater if not too far from floe edges and sustain high biomasses of algae (Ackley et al., 2008). Rafting and ridging of sea ice due to converging floes can also produce seawater-filled gaps that promote ice-algal growth (e.g., Hegseth & Von Quillfeldt, 2002). In addition, rafting and ridging can relocate top and bottom algal communities to the interior of sea ice (Meiners et al., 2012). Very high ice algae biomasses are also observed in sub-ice platelet layers (SIPLs; Arrigo et al., 2010; Dieckmann et al., 1986). SIPLs originate within the range of deep glacial-melt waters, for example, ice shelf water (ISW; Jacobs et al., 1985). When these deep waters are colder than the freezing point of the overlying water, shoaling can form small frazil ice crystals (Jordan et al., 2015). Frazil can grow into ice platelets en route to or in situ beneath sea ice where the platelets may form SIPLs (Langhorne et al., 2015). ISW and SIPLs are common around Antarctic coastal sites (Hoppmann et al., 2020; Langhorne et al., 2015). However, ISW is mostly a late autumn to early spring feature, while unconsolidated SIPLs can be either incorporated by congelated sea-ice growth as platelet ice or redistributed and/or melted in later seasons (Jeffries et al., 1993; Mahoney et al., 2011). As sea ice cools in autumn, assemblages in gaps as well as SIPL communities are frozen and incorporated into the sea-ice cover (Günther & Dieckmann, 1999), and brine inclusions are reduced to pockets again (e.g., Fritsen et al., 1994).

The Indian and Pacific Sectors off East Antarctica harbor about one quarter of the Antarctic sea-ice cover (Parkinson, 2019). Between 69.2% and 91.4% of this sea ice is free-drifting pack ice (Fraser et al., 2012). Pack ice in summer harbors only marginally less algal biomass than its landfast sea ice (fast ice) counterpart (mean 12.9 mg/m^2 vs. 14.5 mg/m^2; Meiners et al., 2012, 2018). According to model and field data, ice algae account for 2%–24% of the total annual primary production in the sea-ice zone (Arrigo, 2017). Seasonally, the contribution from ice algae is only slightly higher in spring than in summer (Arrigo, 2017). This makes summer pack ice
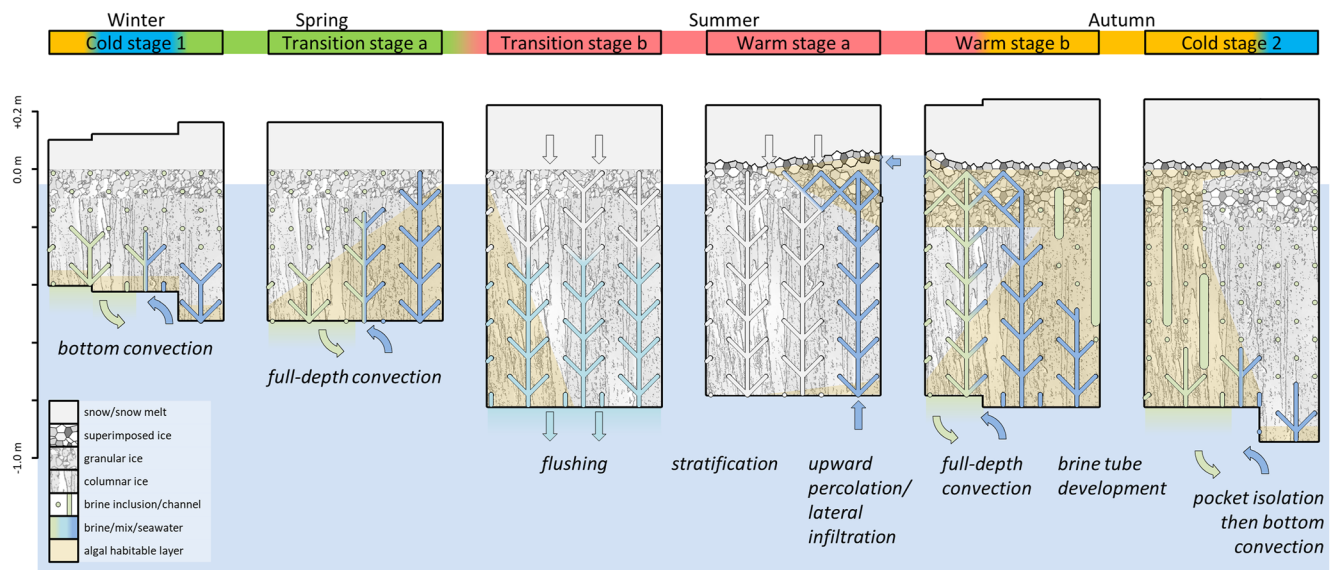
Figure 1. Conceptual model of the thermodynamic temporal evolution of the internal structure of Antarctic sea ice, including pack ice data where possible. Internal structure data from: (1) Zhou et al. (2013; first-year fast ice), (2) Tison et al. (2008; first-year pack ice), (3) Kawamura et al. (2004; first- and multiyear pack ice), (4) Fritsen et al. (1994; multiyear pack ice) and (5) Tison et al. (2017; first-year pack ice). Where these studies contribute to this evolution is given in Table S1 in Supporting Information S1. Sea ice and snow thickness estimates follow data from Worby et al. (2008), Lytle and Ackley (1996), Wadhams et al. (1987) and Tison et al. (2008). Warm stage b and Cold stage 2 would also apply to newly formed first-year ice, with alternation of the two stages depending on synoptic conditions (Tison et al., 2017). Similar behavior could also be observed during Transition stage a, in early spring and at locations of high precipitation and flooding (Lewis et al., 2011). The green unbranched vertical features in the last two stages represent brine tubes (Tison et al., 2017).

an important habitat for primary production, and ice algae an important resource for Antarctic grazers (Bluhm et al., 2010; Caron et al., 2017).

This study describes physical and biogeochemical properties of East Antarctic fast ice and pack ice as observed during austral summer. The state of sea ice in this region at that time may be representative of sea ice under future warming. The aims of this study are to (a) describe the sea-ice structure (ice crystals, brine inclusions and gaps) and how it influences the distribution of ice-algal communities, (b) identify drivers of the sea-ice structure (convergence-driven deformation and crystals that formed due to glacial melt), and (c) evaluate the importance of physical sea-ice properties in driving biogeochemical processes in summer sea ice at an advanced melt phase.

2. Materials and Methods

2.1. Study Area, Field Measurements and Sample Collection

Sea ice was sampled around Wilkes Land and George V Land, East Antarctica, during *RSV Aurora Australis*' Voyage 2 2016–2017 (AAV2 2016–2017, 65°–67°S, 109°–148°E) in austral summer (18 Dec 2016–13 Jan 2017). A 0.14 m internal diameter trace-metal clean electropolished stainless steel corer (Lichtert Industries, Belgium) was used to extract ice cores. To minimize brine loss, cores were immediately cut into 0.1 m sections using a clean stainless steel saw and stored in sealed acid-cleaned plastic buckets. These were transferred to the ship where the ice was melted at room temperature in the dark before analyses. Additional complete cores were extracted (stored horizontally at −20°C) for later ice texture analysis. Brine samples were collected from sack holes ~1 m deep (Miller et al., 2015), and surface-seawater samples were collected either in full-ice-depth bore holes or beside floes (see Table S2 in Supporting Information S1 for additional details).

Samples were collected from two fast ice (Casey1 and Casey2, ~90 m apart in O'Brien Bay) and seven pack ice stations during AAV2 2016–2017 (Figure 2). Stations near the Moscow University Ice Shelf and the Mertz Glacier Tongue, Totten1 and Mertz1, respectively, were identified as broken out fast ice and classified as pack ice. The Dalton and Mertz polynyas where these floes were located are areas of open water that occur north of the Moscow University Ice Shelf and Mertz Glacier Tongue, respectively. Most of the stations appeared to be first-year sea ice as they were relatively thin and undeformed (Figure 2 and Figure S1 in Supporting Information S1). Casey3 was a thick, heavily rafted floe suspected to be multiyear ice. Cores were obtained for measurements of temperature,
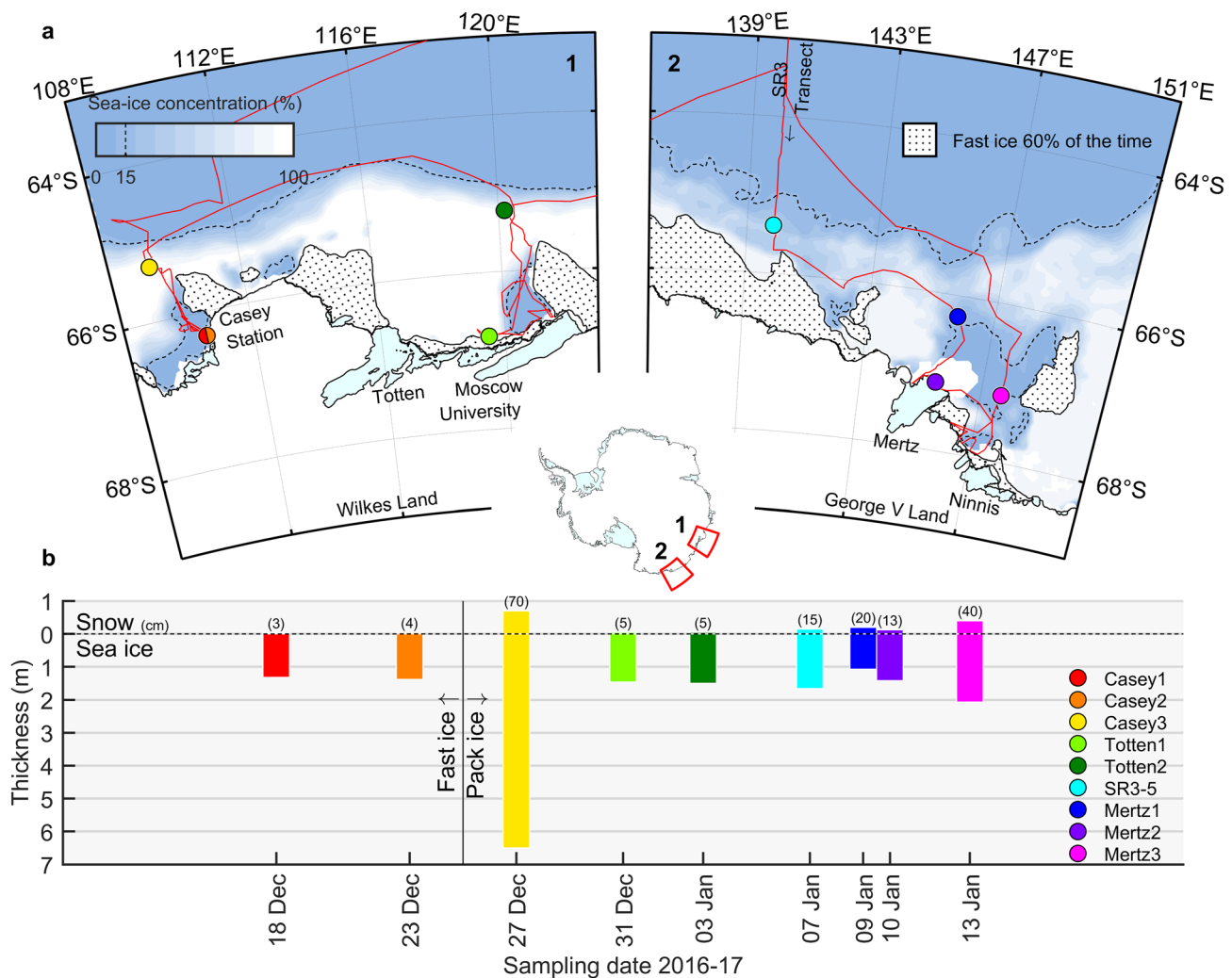
Figure 2. (a) Maps of study area showing voyage track as a red line, mean sea-ice concentration 18 December 2016–13 January 2017 (Spreen et al., 2008) and fast ice which includes icebergs (Fraser et al., 2020; dotted). (b) Sample dates and sea-ice (m) and snow thicknesses (annotated in cm) for stations. Dashed black line indicates snow/sea-ice interface.

salinity and stable oxygen isotopes (physico-chemical); macro-nutrients, chlorophyll *a* (chl *a*) and phaeopigments; and ice textures. Six to seven ~0.1 m sections were analyzed for each macro-nutrient, chl *a* and phaeopigment core. Ice texture cores were only collected from stations Casey1, Totten1, Totten2, SR3-5 (named for its proximity to a nearby long-term hydrography transect station), Mertz1 and Mertz2.

2.2. Sample Processing and Data Analyses

2.2.1. Back and Forward Trajectories and Divergence

Starting from the sampling location of each floe, backward motion trajectories were used to determine the provenance of each ice floe sampled during AAV2 2016–2017, and forward trajectories were used to understand their fate, following Tison et al. (2020). Using a data set of AMSR-2 maximum cross correlation-derived sea-ice motion vectors (Kimura, 2004), floes were advected with the nearest-neighbor velocity. A comparison between velocities used for Kimura's sea-ice motion vectors and velocities derived from buoys in the Ross and Weddell seas had a root mean square deviation of 2.0–5.0 km/day eastward and 2.6–4.4 km/day northward (Tian et al., 2022). In the case of missing data, the mean velocity field of up to eight nearest neighbors was substituted. Trajectories were truncated under three different conditions: (a) when they made contact with a coastal mask which included fast ice (i.e., intercepted stationary features), (b) when there was missing data and no neighbors with which to calculate a substitute, or when they encountered <10% mean sea-ice concentration within 0.6°

latitude and 1.2° longitude from the daily location for the present and two following days (i.e., likely melted/formed), or (c) when they ran for more than 200 days (further tracking became unreliable). The sea-ice motion vectors were also used to calculate daily sea-ice divergence at each floe. Using the four nearest neighbors, the discrete partial derivative of x and y velocities were added together to calculate the divergence. A 5-day-centered moving mean was calculated to smooth the divergence data. Positive divergence creates areas of open water while negative divergence (convergence) collides and deforms sea ice when ice concentrations are very high, possibly resulting in the formation of seawater-filled gaps.

2.2.2. Ice Textures

Five mm thick vertical sections of approximately 0.1×0.1 m were cut from sea-ice cores from Casey1, Totten1, Totten2, SR3-5, Mertz1 and Mertz2 in a $-20°C$ freezer laboratory. These were thinned to approximately 0.5 mm using a microtome (Leica, Germany) and photographed between crossed polarising filters which resolved ice-crystal boundaries and textures (Langway, 1958). Classification of superimposed ice followed Kawamura et al. (2004), as well as Eicken and Lange (1989), whose description of intermediate columnar/granular (c/g) ice was also followed. Classification of platelet ice followed descriptions by Dempsey and Langhorne (2012) and Jeffries et al. (1993).

2.2.3. Temperature and Salinity

Immediately after core recovery, temperature measurements were made in holes drilled ~0.05 m deep every ~0.10 m along a core using a calibrated probe (Testo Pty Ltd, Australia; accuracy: ±0.1°C). This core was cut into 0.1 m vertical sections and melted. Salinity samples were analyzed on the ship using a Guildline Autosal 8400B salinometer (Ocean Scientific International Ltd, United Kingdom; accuracy: ±0.01) in a constant temperature laboratory to prevent instrument drift. The temperature data were used to calculate brine salinity (S_{br}^{POLY3}), which was used to identify brine stratification, following Vancoppenolle et al. (2019):

$$S_{br}^{POLY3} = -18.7T - 0.519T^2 - 0.00535T^3, \tag{1}$$

where T is temperature (°C). With the addition of salinity data, the brine volume fraction (ϕ_{br}^v) was also calculated following Vancoppenolle et al. (2019):

$$\phi_{br}^v = \left[1 + (1/\phi_{br} - 1)\rho_{br}/\rho_i\right]^{-1}, \tag{2}$$

where ϕ_{br} is the mass fraction of brine and ρ_{br} and ρ_i are the brine and pure ice densities, calculated following Zubov (1945) and Pounder (1965) as per Vancoppenolle et al. (2019) and Cox and Weeks (1983). As air volume fractions can be crucial in old ice, especially in the freeboard, herein we refer to what is termed ϕ_{br}^v in the above equation as porosity, which is the combined air and brine volume (Timco & Weeks, 2010; Vancoppenolle, Notz, et al., 2013).

2.2.4. Stable Oxygen Isotopes

The ratio between the ^{18}O and ^{16}O isotopes in sea ice is given by $\delta^{18}O$, where the sample ratio is compared to an ocean water standard (Brandon et al., 2010). Sea-ice $\delta^{18}O$ is classically used to differentiate meteoric-origin ice (more negative) and frozen seawater (more positive; e.g., Worby & Massom, 1995). Sea ice with a meteoric signature includes snow ice, superimposed ice and ice platelets grown with deep glacial-melt input. The $\delta^{18}O$ of bulk sea ice is commonly between 0 and +3‰ due to little fractionation during fast freezing and enrichment of ^{18}O in the ice during slow freezing (Eicken, 1998).

Sea-ice $\delta^{18}O$ related to Standard Mean Ocean Water was measured from 0.10 m vertical ice-core sections using an ISOPREP-18 equilibration bench and a SIRA dual-inlet mass spectrometer (VG Isogas Ltd, United Kingdom; accuracy: ± <0.05‰) at the University of Tasmania's Central Science Laboratory in Hobart, Australia. For the fast ice stations, the $\delta^{18}O$ of brine was estimated with the following mixing equation (developed in Text S1 in Supporting Information S1):

$$\delta^{18}O_{br} = \frac{\delta^{18}O_{si} - \delta^{18}O_i\left(1 - \phi_{br}^v\right)}{\phi_{br}^v}, \tag{3}$$

where $\delta^{18}O_{br}$, $\delta^{18}O_i$ and $\delta^{18}O_{si}$ are brine, pure ice and bulk sea ice, respectively. A value of +2.63‰ was used for $\delta^{18}O_i$, as calculated by Eicken (1998) for the pure ice fraction of 7% porous sea ice at the slowest realized growth

rate. Fixing the $\delta^{18}O_i$ at a value for slow growth, while simple, may cause $\delta^{18}O_{br}$ to be underestimated, especially in upper ice where freezing could have been fast. $\delta^{18}O_{br}$ was used to estimate the proportion of melted snow in the brine (ϕ^{br}_{snow}) with the following dilution equation (developed in Text S2):

$$\phi^{br}_{snow} = \frac{\delta^{18}O_{br} - \delta^{18}O_{mix}}{\delta^{18}O_{snow} - \delta^{18}O_{mix}} \cdot 100,$$

(4)

where $\delta^{18}O_{mix}$ is a mixture of residual brine from freezing, non-snow melt and seawater, $\delta^{18}O_{snow}$ is snow, both $\delta^{18}O_{mix}$ and $\delta^{18}O_{snow}$ mix to give $\delta^{18}O_{br}$. We expect that $\delta^{18}O_{mix}$ for brine should be somewhere between -3 (overwhelmed by residual brine from freezing) and $+3‰$ (overwhelmed by slow-frozen sea-ice melt) with $0‰$ seawater. On the other hand, $\delta^{18}O_{snow}$ is commonly between -15 and $-25‰$ (Worby & Massom, 1995). A short-coming of this method is that neglected melt from snow derivatives (i.e., snow ice and superimposed ice) would lower the actual $\delta^{18}O_{mix}$ and result in overestimated ϕ^{br}_{snow}. To test for sensitivity, ϕ^{br}_{snow} was calculated with $\delta^{18}O_{mix}$ and $\delta^{18}O_{snow}$ at -3 and $+3‰$, and -15 and $-25‰$, respectively.

2.2.5. Macro-Nutrients

Unfiltered macro-nutrient samples of melted ice-core sections were stored at $-20°C$ before being analyzed at the Commonwealth Scientific and Industrial Research Organisation (CSIRO) laboratory in Hobart, Australia. An AA3 segmented flow instrument (SEAL Analytical Ltd, United Kingdom) was used to determine concentrations of nitrate + nitrite (NO_x) following Wood et al. (1967), silicic acid ($Si(OH)_4$) following Armstrong et al. (1967), phosphate (PO_4^{3-}) following Murphy and Riley (1962), and ammonia (NH_3) following Kérouel and Aminot (1997) (accuracy: ± 0.02 μM for reactive nitrate, phosphate and ammonia; ± 0.01 μM for reactive nitrite; ± 0.20 μM for reactive silicic acid; Rees et al., 2019).

Salinity-normalized $Si(OH)_4$ in melted sea ice, brine from sack holes and seawater were calculated following Fripiat et al. (2017). These authors found that winter seawater macro-nutrient concentrations approximated salinity-normalized macro-nutrient concentrations in winter sea ice. The Antarctic Remote Ice Sensing Experiment (ARISE, October 2003, 63–66°S, 109–118°E) was geographically close to AAV2 2016–2017 and was the nearest to a winter study available. Thus, the median concentration of $Si(OH)_4$ in seawater from ARISE was used here as the theoretical winter stock in sea ice (Becquevort et al., 2009; Lannuzel et al., 2007).

2.2.6. Chlorophyll *a* and Phaeopigments

Chlorophyll *a* and phaeopigments (which are degradation products of chlorophyll) were used to assess biomass and the health of algal assemblages, respectively (Arrigo et al., 2014). Sea-ice samples for pigment analysis were only handled in the dark and filtered immediately after melting within 24 hr. Sea-ice melt was filtered onto 25 mm diameter GF/F filters (Whatman, United Kingdom) and pigments were extracted from filters in 90% acetone in the dark at $-20°C$ for 24–48 hr (Holm-Hansen et al., 1965; Lorenzen, 1966). Chl *a* and phaeopigments were measured with a Turner Trilogy fluorometer (Turner Designs, United States of America; accuracy: ± 0.025 μg/L) during the voyage. The ratio of phaeopigments to total chlorophyll pigments (degraded and non-degraded) was calculated to assess algal community health, similar to Tison et al. (2017).

2.3. Statistical Analysis

For analyses of variance and correlations, the Shapiro-Wilk test was used to check whether variables had normal distributions. For variables with non-normal distributions the following non-parametric analyses were undertaken. The Kruskal-Wallis test was used to test for differences in macro-nutrient concentrations as well as chl *a*, for different ice textures as well as between different ice porosities. A deformed ice classification was added to the ice texture analyses for natural core breaks and thermodynamic growth disruptions. Additionally, Spearman's correlation tests were performed between ice porosity and macro-nutrients as well as chl *a*.

3. Results

3.1. Back and Forward Trajectories and Divergence

Casey1, Casey2 and Totten1, were within the coastal mask of the coarse daily motion product, hence our back-tracking method could not resolve any advection. The remaining floes could be traced back between 42 and
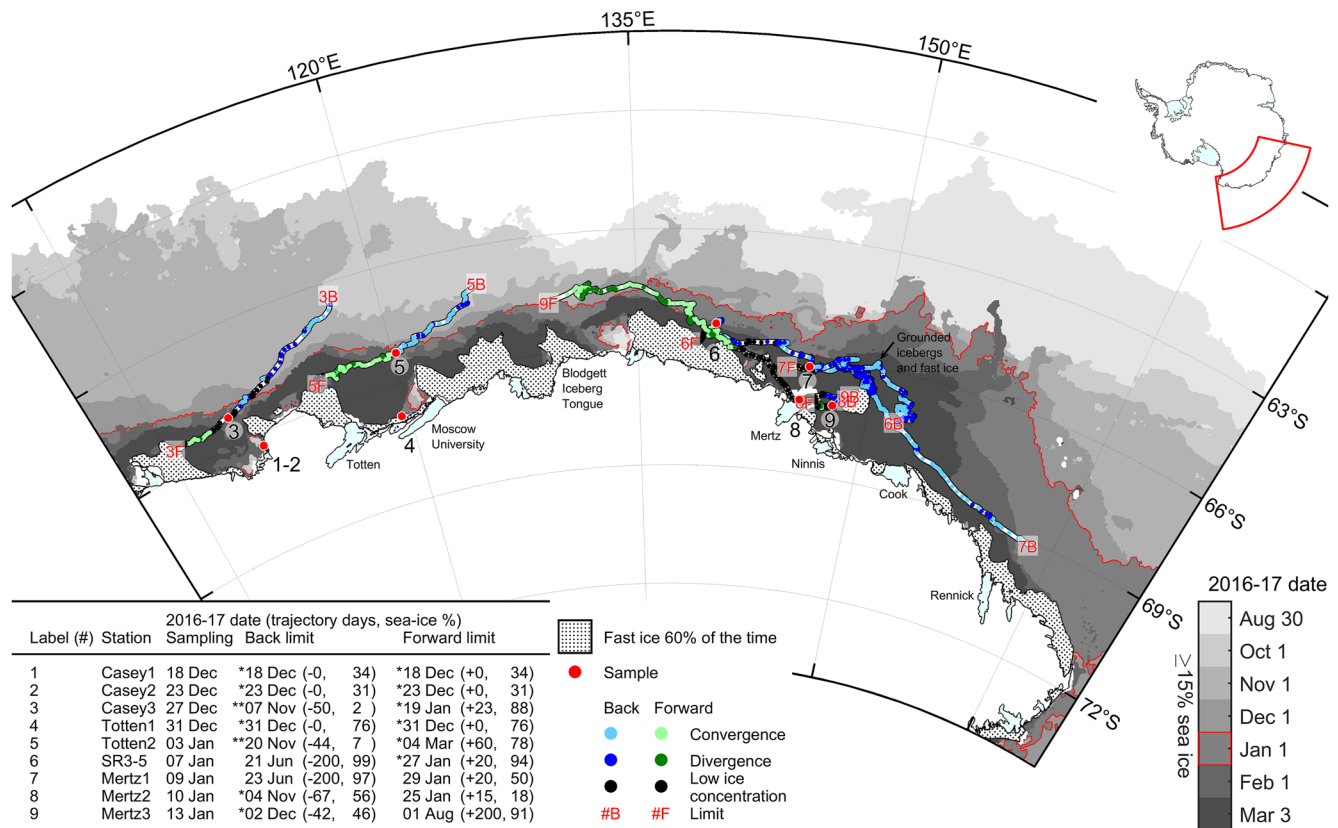
Figure 3. AAV2 2016–2017 sampling area around Wilkes Land and George V Land with sampled ice floe forward and backward trajectories colored by 5-day-centered moving mean divergence. Ice shelves are overlaid on the coastline in cyan (Greene et al., 2017; Mouginot et al., 2017; Rignot et al., 2013). Fast ice data are from 2000–2014 except for the Mertz region where 2016–2017 data was inserted (Fraser et al., 2020), the 60% time contour was used as it best resolved features such as iceberg tongues. Periodic sea-ice edges (15% contour) derived from AMSR-2 are indicated by filled greyscale contours (Spreen et al., 2008). Single asterisks denote trajectories terminated early due to intercepting the coastal mask which includes fast ice. Double asterisks denote trajectories terminated early due to continuous low sea-ice concentration.

200 days (mean 100.5 ± 77.6 days; herein all means are shown with ± one standard deviation) and 110 and 1,577 km (mean 705 ± 602 km; Figure 3). The Mertz1 floe spent 20.5% of its back trajectory less than 80 km from the coast, passing within ~50 km of the Cook Ice Shelf before skirting around the northern tip of an iceberg and fast ice conglomerate (Figure 3). Mertz2 and Mertz3 likely originated from near the conglomerate of fast ice and grounded icebergs on the Ninnis Bank (which Mertz1 skirted around). Forward tracking was between 15 and 200 days (mean 56.3 ± 72.3 days) and 59 and 1,510 km (mean 397 ± 557 km; Figure 3). The forward trajectories of Casey3, Totten2 and SR3-5 floes all terminated in fast ice. Mertz1 and Mertz2 appeared to melt in January 2017.

3.2. Snow and Ice Textures

Snow thicknesses were between 0.03 and 0.7 m (mean 0.19 ± 0.22 m; Figure 2b). Snow loads were mostly old with large melted and refrozen crystals, with the exception of Casey2 where snow was fresh. Freeboards were all positive, that is, snow/ice interfaces were all above sea level. The ice textures of all the examined cores included superimposed (3.8%), small granular (54.3%), intermediate c/g (4.3%), columnar (28.6%) and incorporated platelet ice (8.1%; Figure 4). The superimposed ice occurred on top of pack ice stations, whereas the fast ice station had intermediate c/g on top (Figure S2 in Supporting Information S1 for zoom). Honeycomb features with large voids of diameters up to 0.02 m were found in the upper ~0.5 m of all the ice cores, indicating internal melt in the upper ice due to absorbed solar radiation. While no texture core was collected, the upper part of the sea ice at Mertz3 was observed to be highly porous and wet and contained ice algae. Platelet ice textures were bladed at Totten1 (0.48–0.91 m) and Mertz1 (0.63–0.68 m) and draped, or wavy-edged, at Mertz2 (1.14–1.30 m) (Figure S3 in Supporting Information S1). Platelet ice was 47% of the ice thickness at Totten1. An alternative description
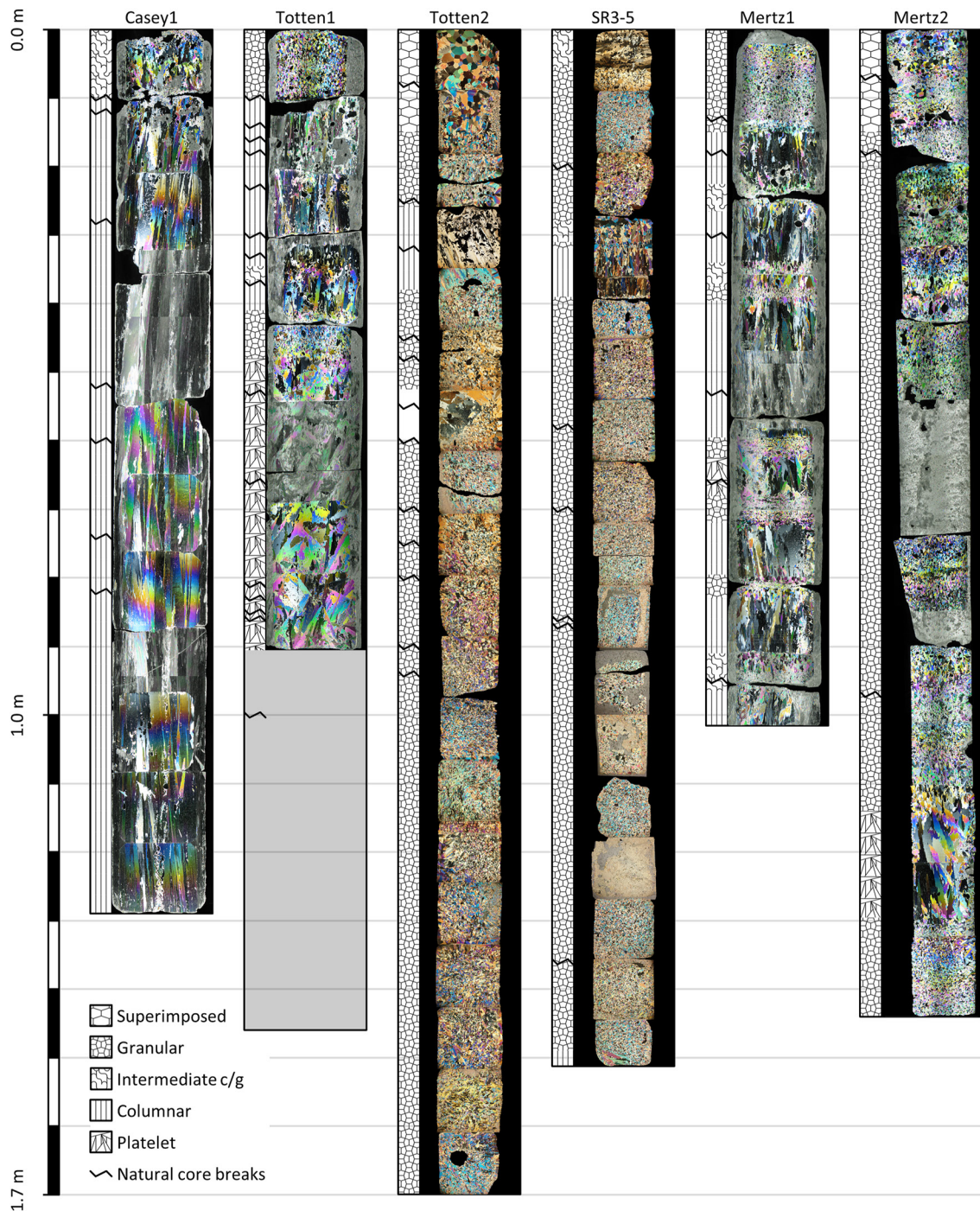
Figure 4. Ice textures from 0.14 m diameter sea-ice cores, c/g stands for columnar/granular. Cores for ice textures were only collected from six of nine stations. Images of thin sections (~0.5 mm) are overlaid on thick sections (~5 mm). The natural core breaks are compiled from all the cores collected at the respective station and could be indicative of internal layers resulting from rafting or the decay of granular ice crystals. Neighboring cores at Totten1 were considerably longer than the texture core (gray box). The Totten2 and SR3-5 cores appear different in color to the other cores because they were processed in a different laboratory.

of our defined platelet ice at Mertz2 might be an under-rafted floe with coarse granular on top of columnar ice, but internal brine layers which should exist in columnar crystals were not apparent.

Totten2 appeared deformed, especially the feature between 0.53 and 0.6 m. Mertz1 columnar ice was interrupted by layers of small granular, intermediate columnar/granular and platelet ice which coincided with natural core breaks. There did not appear to be any strong indicators of rafting such as unusual crystal orientations or
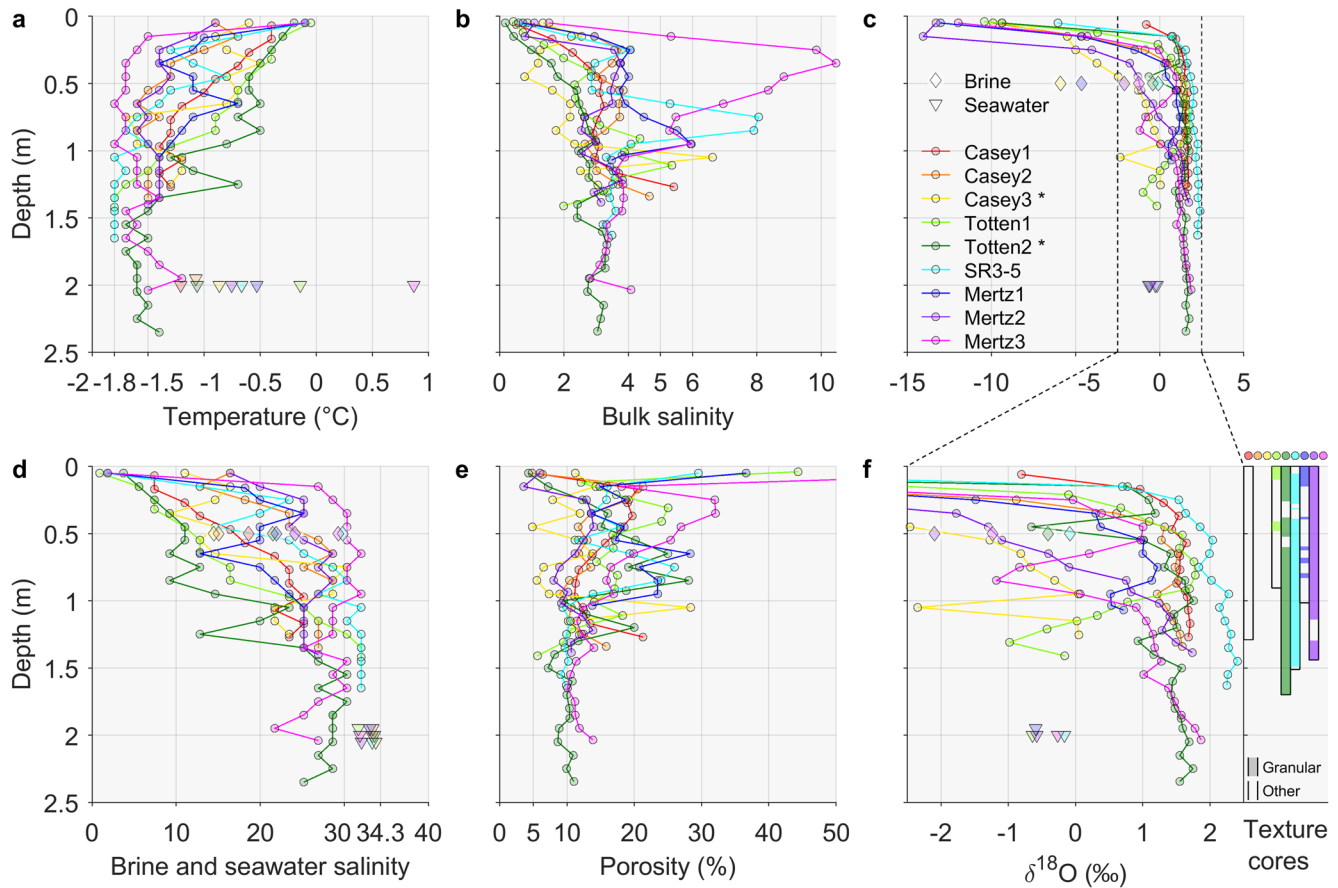
Figure 5. Depth profiles of sea-ice-core (a) temperature, (b) bulk salinity, (c) stable oxygen isotope ratios (δ^{18}O), (d) brine salinity with markers showing seawater salinity, (e) porosity (non-solid ice fraction) and (f) δ^{18}O with the *x*-axis magnified relative to (c). Granular ice textures are plotted alongside in panel (f) to show where granular ice coincides with negative δ^{18}O. Where applicable and where data were collected, brine measurements (diamonds) are scattered at 0.5 m and seawater measurements (triangles) are scattered at 2.0 m. Asterisks after station names denote ice cores that were not full-ice-depth.

mylonitisation zones, which disrupt the original ice texture with mechanical forces applied in the direction of rafting (Eicken & Lange, 1989; Lange et al., 1989). However, these features, and thus deformation, may be difficult to discern in fine-grained granular ice.

3.3. Temperature and Salinity

Sea-ice temperatures at the time of core extraction were between −1.8 and 0.0°C (mean −1.2 ± 0.5°C; Figure 5a). Of the pack ice, Mertz2 had the coldest top-ice temperature at −0.9°C. The mean of air temperatures measured on-board the ship during the 3 hours prior to sampling of Mertz2 was also the coldest at −2.6°C, while air temperature at the other pack ice stations ranged from −2.1°C at Mertz3 to +0.4°C at Casey3. Seawater temperatures ranged from −1.2°C at Casey1 to +0.9°C at Mertz3. Sea-ice bulk salinities were between 0.2 and 10.5 (mean 3.3 ± 1.7; Figure 5b). Calculated brine salinities ranged from 0.9 to 32.0 (mean 22.2 ± 8.1; Figure 5d), mostly increasing with depth and lower than the salinity of the underlying seawater (mean 32.9 ± 0.8; Figure 5d). Calculated sea-ice porosities were between 3.6% and 80.8% (mean 15.0 ± 8.6), mostly greater than 5% and often greater than 10% (Figure 5e). Top-ice (0–0.1 m) values at Totten1, SR3-5 and Mertz1 exceeded 29.5% while Mertz3 was 80.8% (off scale in Figure 5e). In contrast, porosities of 4.2% and 3.6% occurred in the upper 0.1 m of Totten2 and between 0.1 and 0.2 m in Mertz2, respectively.

3.4. Stable Oxygen Isotopes

Sea-ice δ^{18}O values were between −14.1 and 2.4‰ (mean −0.1 ± 3.2‰; Figures 5c and 5f). Underlying seawater δ^{18}O values were between −0.6 and −0.2‰ (mean −0.4 ± 0.2‰). Except for sea ice at Casey1 and SR3-5 which
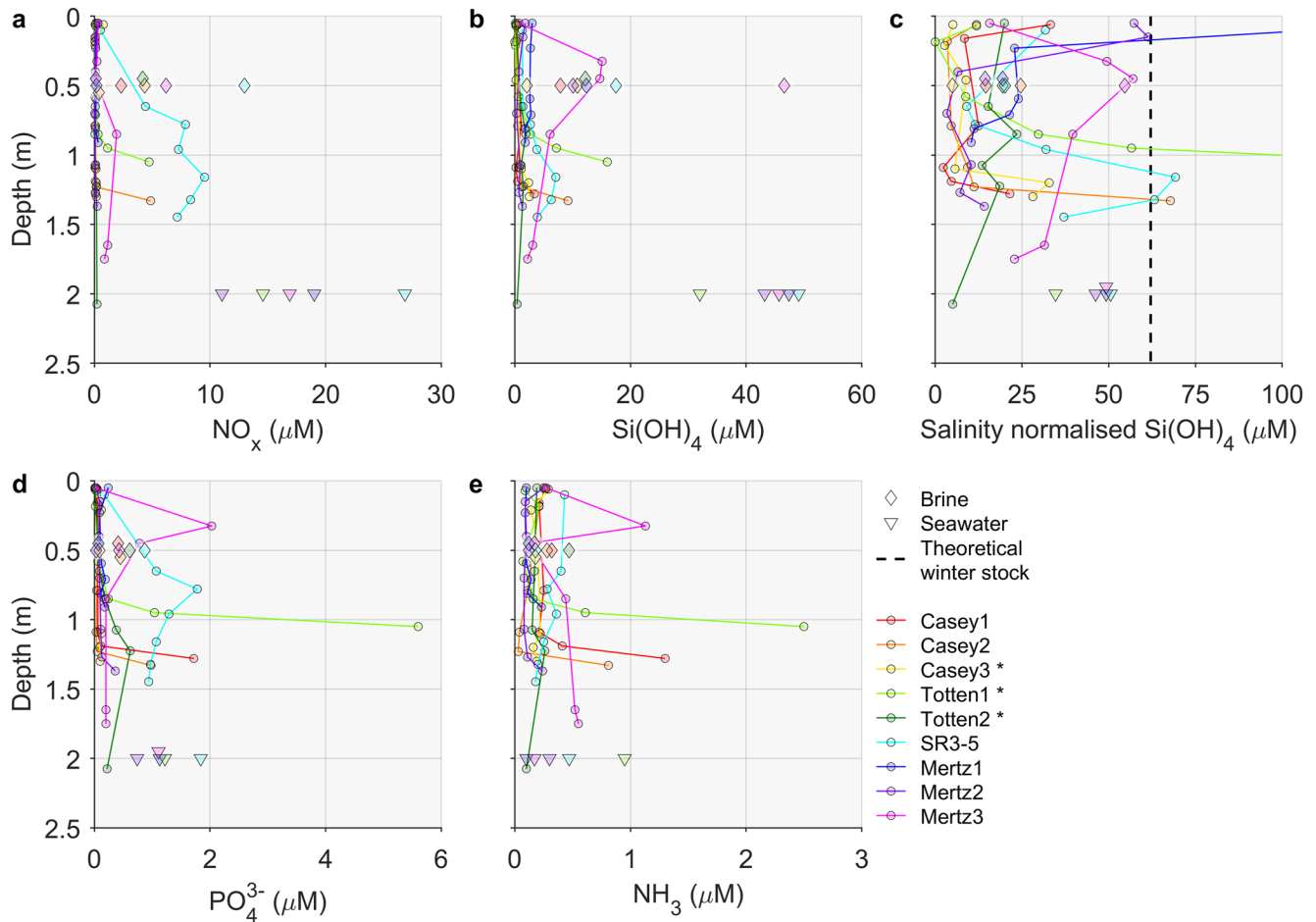
Figure 6. Depth profiles of sea-ice-core (a) nitrate + nitrite (NO_x), (b) silicic acid ($Si(OH)_4$), (c) salinity-normalized $Si(OH)_4$, (d) phosphate (PO_4^{3-}) and (e) ammonia (NH_3) concentrations. Where data were collected, brine measurements (diamonds) are scattered at 0.5 m and seawater measurements (triangles) are scattered at 2.0 m. The theoretical winter stock of $Si(OH)_4$ is given by a dashed black line in (c). Asterisks after station names denote ice cores that were not full-ice-depth.

were −6.1 and −0.8‰, respectively, top-ice values were between −14 and −9‰. Values increased to those close to underlying seawater within the upper 1 m for Casey3 and Mertz2 and within the upper 0.5 m for the remaining stations.

3.5. Macro-Nutrients

The mean concentrations of sea-ice macro-nutrients were 1.18 ± 2.42 μM for NO_x, 2.64 ± 3.62 μM for $Si(OH)_4$, 0.44 ± 0.86 μM for PO_4^{3-} and 0.30 ± 0.38 μM for NH_3. There were macro-nutrient peaks at the bottom of the fast ice cores and in the interior of Totten1, SR3-5 and Mertz3 (Figure 6). Except for peaks at the top of Mertz1, in the interior of Totten1 and SR3-5, and at the bottom of Casey2, salinity-normalized $Si(OH)_4$ was less concentrated than the calculated theoretical winter stock (Figure 6c). Comparison with theoretical winter stocks for the remaining macro-nutrients showed considerable enrichment for PO_4^{3-} and NH_3 (Figure S4). Nitrate + nitrite was only enriched in the sections of Casey2, Totten1 and SR3-5 with high concentrations of chl *a* (see Section 3.6), coincident with peaks in the raw macro-nutrient data.

Compared to bulk ice, mean concentrations of macro-nutrients in brine samples were higher for NOx (3.84 ± 4.32 μM) and $Si(OH)_4$ (15.0 ± 13.5 μM) and lower for PO_4^{3-} (0.37 ± 0.29 μM) and NH_3 (0.23 ± 0.12 μM). Brine and underlying seawater concentrations of $Si(OH)_4$ at Mertz3 were very similar at 46.6 and 45.7 μM, respectively. The mean bulk ice NH_3 was comparable to underlying seawater (0.40 ± 0.34 μM). In contrast, bulk ice NO_x, $Si(OH)_4$ and PO_4^{3-} were generally less concentrated than the underlying seawater (17.67 ± 5.92 μM, 43.5 ± 6.8 μM and 1.21 ± 0.40 μM, respectively). Seawater medians were mostly lower than those from the ARISE cruise, except for NH_3 which was considerably higher (Table S3).

3.6. Chlorophyll *a* and Phaeopigments

Chlorophyll *a* concentrations in sea ice ranged from 0.1 to 92.3 µg/L (mean 13.5 ± 21.8 µg/L), while seawater and brine chl *a* values were between 0.4 and 6.2 µg/L and 0.4 and 5.9 µg/L, respectively (Figure 7). The highest chl *a* concentrations were found in bottom algal assemblages at the fast ice stations Casey1 and Casey2. Totten1 had a similarly high chl *a* signal in its interior. Internal algal assemblages were also found at Totten2, SR3-5 and Mertz3. Phaeopigment to total chlorophyll pigment percentage contributions were between 8.0% and 60.9% (mean 29.5 ± 11.7%). The minimum values across the Mertz stations were between 21.6% and 28.4%, while the minimums of the remaining stations were between 8.0% and 19.0%. Maximum values exceeded 50% in the brine at Casey3 (72.9%), in the upper 0.20 m of Totten1 (50.1%–57.4%), above the internal assemblage at Totten2 (50%), at the top of SR3-5 (55.8%), and at the top and in the underlying seawater of Mertz3 (60.9% and 53.3%, respectively).

3.7. Macro-Nutrient and Chlorophyll *a* Relationships With Ice Textures and Porosities

All the variables tested had non-normal distributions (Shapiro-Wilk test $p < 0.05$) so further analyses were non-parametric. While there were instances of high macro-nutrient concentrations matching the highest chl *a* values in deformed ice (of measurements coincident with ice textures, Figure S4 in Supporting Information S1), concentrations of macro-nutrients and chl *a* were not significantly different between the different ice textures listed in Section 3.2 with the addition of deformed ice (Kruskal-Wallis test $p > 0.05$; Table S4 in Supporting Information S1). Nor were they significantly different between ice porosities less than or equal to 30% divided into 5% bins (Kruskal-Wallis test $p > 0.05$). There was, however, a general trend of relatively low macro-nutrient and chl *a* concentrations in the 0%–5% porosity bin compared to the 5%–30% porosity bins (Figure S5 in Supporting Information S1). Spearman correlations between macro-nutrients as well as chl *a* and ice porosity were also not significant ($p > 0.05$), but the correlation coefficients were all positive (Table S4 in Supporting Information S1), in agreement with the general trend of increasing macro-nutrients and chl *a* with increasing porosity up to 30% porosity.

3.8. Surface Melting

A surface pond was sampled at Totten1 (Figure S6 in Supporting Information S1). The salinity of the surface pond was 5.5, which corresponded to the brine salinity calculated for just below the top of the ice, and the $\delta^{18}O$ was −4.7‰. Some brine sack hole $\delta^{18}O$ values were similarly low, with a minimum of −5.9‰, which suggests snow meltwater entrainment (−5‰ threshold; Eicken, 1998). In addition, negative $\delta^{18}O$ values were found in non-granular ice at Casey1, Totten1 and Mertz1 (Figure 5f). Bulk sea-ice $\delta^{18}O$ at the top of Casey1 was −0.8‰ even though the textures were not characteristic of refrozen snow. Interior sections (below the upper 0.1–0.2 m, where there may have been interposed ice) of the fast ice stations were the most suitable for assessing snowmelt contribution to brine (Table 1). The sampled ice was not deformed in O'Brien Bay (Casey1 and 2; Figure S1 in Supporting Information S1), while the pack ice stations were likely heavily influenced by meteoric ice as they had characteristics of either: superimposed ice, rafting (i.e., may have had internal layers of snow ice; Casey3, Totten2 and SR3-5), mostly granular with an indeterminably thick layer of snow ice (Mertz2), or contained layers of frazil or platelet ice (Totten1, Mertz1 and Mertz2). $\delta^{18}O_i$ was kept constant at +2.63‰ in Equation 3 as decreasing this value (increasing the ice-growth rate) soon resulted in negative ϕ^{br}_{snow} values when $\delta^{18}O_{mix}$ was also decreased.

3.9. Internal Layers

Relatively warm and/or salty, high-porosity internal layers occurred in the sea ice at Casey3, Totten2, SR3-5, Mertz1 and Mertz3 (Figures 5a, 5b and 5e). These layers coincided with both $\delta^{18}O$ troughs and macro-nutrient peaks (Figures 5f and 6). Figure 8 highlights some of these layers at Totten2 and SR3-5. Mertz3 had a $Si(OH)_4$ peak of 15.1 µM between 0.25 and 0.4 m. SR3-5's NO_x and PO_4^{3-} were relatively high below the top at ~8 µM and peaking at 1.78 µM, respectively. Ammonia peaks often coincided with peaks of other macro-nutrients. Internal assemblages all coincided with these high-porosity layers (Figure 7).
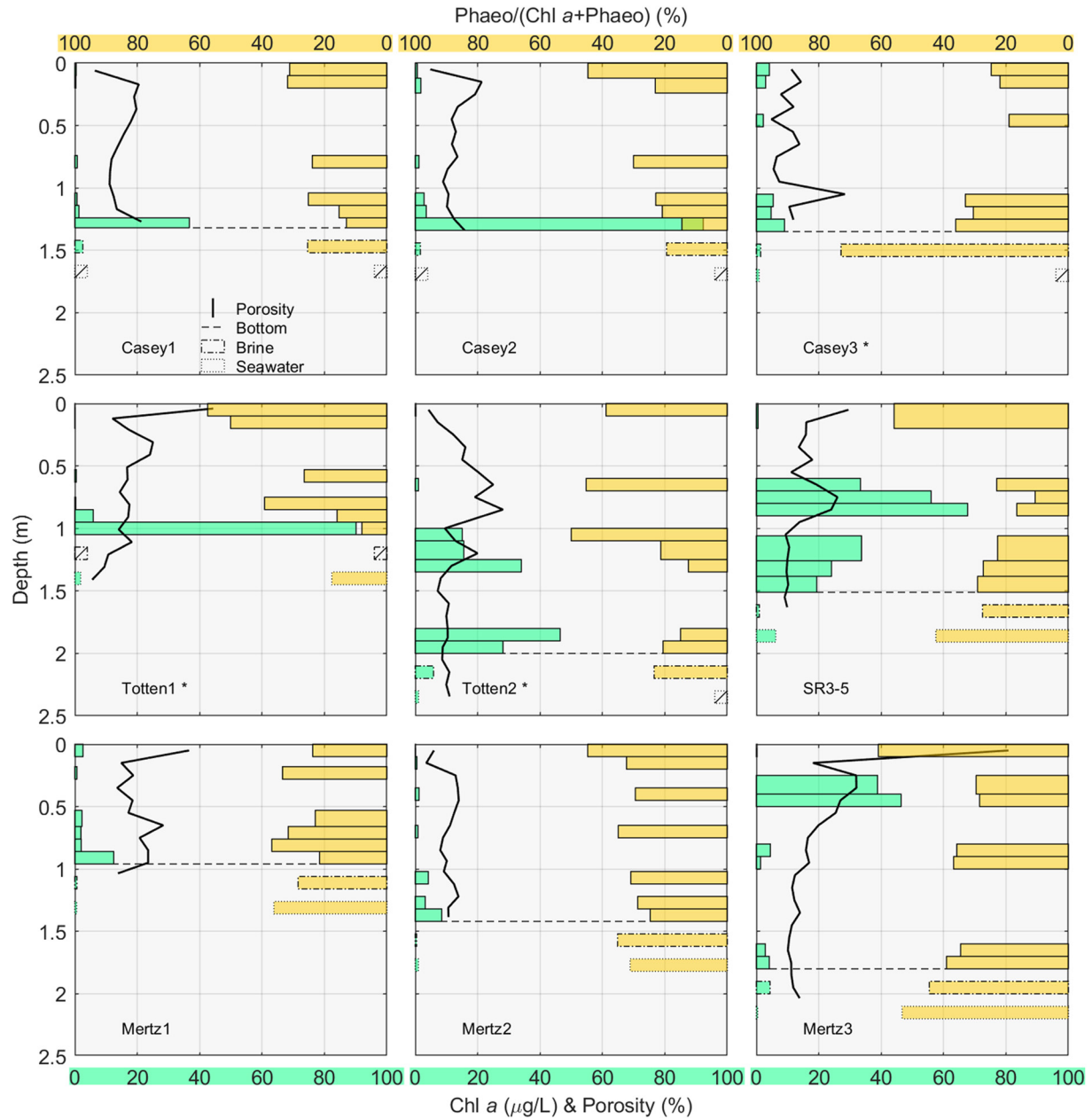
Figure 7. Depth profiles of sea-ice core chlorophyll *a* (chl *a*) concentrations and phaeopigment to total chlorophyll pigment (degraded and non-degraded) percentage contributions. Where data were collected, brine and seawater measurements are shown below sea-ice measurements. Seawater chl *a* at Casey3 and Totten2 are mean (*n* = 3) shipboard measurements around the ∼6 hr of sampling. Asterisks after station names denote ice cores that were not full-ice-depth. Depth profiles of sea-ice porosity are given by solid black lines.

4. Discussion

4.1. Rotten Ice

The East Antarctic sea ice sampled for this mid-summer study was rotten, heavily melted and disintegrated, riddled with melt holes (honeycombed) and highly permeable (as defined by: Frantz et al., 2019; World Meteorological Organization, 2014). The texture cores and field observations identified honeycombed ice with extensive brine networks and large brine channels. The mean porosity of 15.0 ± 8.6% (i.e., a solid ice fraction of 85%) surpasses the 5% and suspected 10% porosity thresholds for percolation of brine through columnar/incorporated platelet and granular ice, respectively (Golden et al., 1998; K. M. Golden, personal communication, 2016;

Table 1
Snowmelt Contributions to Brine (ϕ_{snow}^{br}) at Fast-Ice Stations Calculated With Equations 3 and 4

	$\delta^{18}O_{snow}$ (‰)	$\delta^{18}O_{mix}$ (‰)	ϕ_{snow}^{br} range (%)	ϕ_{snow}^{br} mean ± SD (%)
Casey1 (0.1–1.3 m depth, $n = 12$)	−25	−3	−5.3* to 19.9	7.9 ± 7.1
		+3	17.3 to 37.1	27.6 ± 5.6
	−15	−3	−9.7* to 36.5	14.5 ± 13.0
		+3	26.9 to 57.7	43.0 ± 8.7
Casey2 (0.2–1.4 m depth, $n = 12$)	−25	−3	4.4 to 57.7	26.7 ± 15.3
		+3	24.9 to 66.7	42.4 ± 12.0
	−15	−3	8.1 to 105.7*	48.9 ± 28.0
		+3	38.7 to 103.8*	65.9 ± 18.7

Note. Sensitivity tested for the bounds of stable oxygen isotope ratios reported for snow ($\delta^{18}O_{snow}$; Worby & Massom, 1995) and the bounds of stable oxygen isotope ratios for the mixture of residual brine from freezing, non-snow melt and seawater in brine ($\delta^{18}O_{mix}$). Values below 0% and above 100% are denoted with asterisks.

Wongpan et al., 2018). Figure 1, the conceptual model for sea-ice evolution, suggests that the sea ice from this study was in a state somewhere between Transition stage b and Warm stage b, which involves the following characteristics, as developed in the following sections: (a) the brine network has been well flushed by surface melt (snow and sea ice) and is stratified, (b) the snowpack has melted and refrozen to form superimposed and interposed ice and (c) snow on top of the sea ice flooded with seawater and refroze into snow ice.
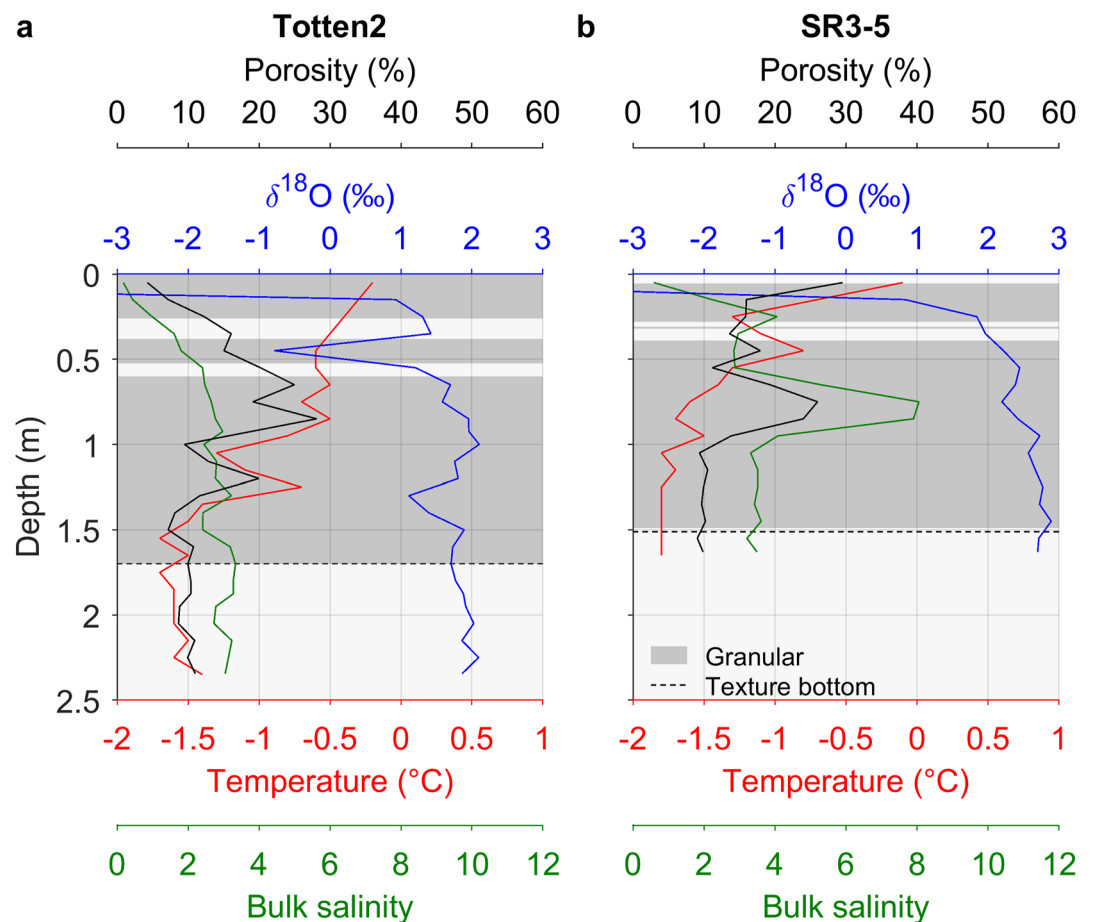

Figure 8. Examples of warm, salty, high-porosity and low $\delta^{18}O$ internal layers at (a) Totten2 and (b) SR3-5. Dashed black line indicates the bottom of the ice-texture core, beyond which textures were unknown. Gray shading represents granular ice textures.

4.1.1. Brine Stratified and Brine Network Well Flushed by Surface Melt

Brine salinity increased with ice depth but remained fresher than the underlying seawater suggesting that melt had mixed with and stratified the brine (Warm stage a in Figure 1). Movement through the brine network should have largely been limited to molecular diffusion (Vancoppenolle et al., 2010). We considered our seawater $\delta^{18}O$ values to be influenced by melted ice and thus not necessarily representative of the seawater from which the sea ice grew. No winter seawater $\delta^{18}O$ measurements were found for Wilkes Land and George V Land, therefore origin seawater was considered $\sim 0‰$ for $\delta^{18}O_{mix}$ in Equation 4. For comparison, in Erebus Bay in July, Toyota et al. (2013) found seawater below sea ice (10 m below water surface) to have $\delta^{18}O$ of $-0.61‰$. While no platelet ice was present when Toyota et al. (2013) collected this seawater, according to seawater temperatures at 200 m depth relative to the surface freezing point this region appears to be more influenced by deep glacial melt than our study region, thus seawater $\delta^{18}O$ could be more negative (Langhorne et al., 2015).

According to $\delta^{18}O$ calculations, snowmelt was entrained in brine at Casey1 and Casey2 to mean proportions of snowmelt as low as $7.9 \pm 7.1\%$ and $26.7 \pm 15.3\%$, respectively (Table 1). At Casey2 snowmelt entrainment reached the bottom of the ice, indicating strong surface-melt flushing of the brine network. Casey2 was sampled less than 100 m from the Casey1 site 5 days later. At this time of year, porosities are very high, and the composition of the brine may change rapidly due to surface-melt flushing. On the other hand, ice growth from a refreezing event which possibly occurred between Casey1 and Casey2 (Casey2 top ice was colder and less porous) could have reinitiated brine convection and smeared the snowmelt $\delta^{18}O$ signal to depth.

4.1.2. Snowpack Metamorphosed Into Superimposed and Interposed Ice

Low porosities (<5%) in the upper 0.10 m of Totten2 and between 0.10 and 0.20 m in Mertz2 coincided with superimposed ice textures. The rottenness of the upper sections of sea-ice cores as well as the 0.10 m vertical resolution may be responsible for masking the low porosities and bulk salinities of superimposed and/or interposed ice layers at other pack ice stations. Totten2 had a thick layer of large ($\sim$5–15 mm) polygonal granular crystals (Figure S2b in Supporting Information S1) resembling the superimposed ice described by Kawamura et al. (2004) for first-year pack ice in the eastern Ross Sea sampled in January. Kawamura et al. (2004) suggested that superimposed ice melts to form surface ponds purely composed of melt (melt ponds), marking the disappearance of the snow cover. However, melt ponds are rare around Antarctica and surface ponds are more often seawater or brine (Andreas & Ackley, 1982; Hudier et al., 1995). We observed several surface ponds including within the ice pack around the Dalton and Mertz polynyas. The surface pond sampled at Totten1, where there was very little snow, more closely resembled the upper sea ice with respect to $\delta^{18}O$ while its salinity more closely resembled the upper brine suggesting that this was not seawater infiltrating a crack in the ice cover (Massom et al., 2001). The surface pond's salinity was also lower than some ponds previously sampled in the Weddell Sea in January, which were mostly formed by flooding from ridge loading (19.4 ± 7.1), supporting that this was likely a true melt pond (Ackley & Sullivan, 1994; Haas et al., 2001).

In the Ross Sea in January 1999, Kawamura et al. (2004) reported superimposed ice layers comparably thick to ours (0.1–0.2 m), which contributed less overall to the ice examined (2.4% vs. our 3.8%). Their snow cover was also intact and no melt ponds were observed, which suggests a more advanced melting of the snowpack sampled during December 2016-Jan 2017 (Morris & Jeffries, 2001). Melt ponds in the East Antarctic ice pack at the time of our study could have provided a pathway for exchange between the underlying seawater, sea ice, and atmosphere at a time when superimposed and interposed ice was otherwise sealing the top of the sea ice (Nomura et al., 2010).

4.1.3. Seawater Infiltrated Top of Sea Ice

Totten1 and Mertz1 appeared to have snow ice at the top, which is indicative of historical surface flooding and refreezing, as in the Warm stages in Figure 1 or even earlier with suitable synoptic conditions (Tison et al., 2017). Although Mertz3 was not sampled for textures, it showed considerable erosion (tens of centimeters horizontally) at the snow/sea-ice interface at the periphery of the floe (Figure S7 in Supporting Information S1). This might suggest historical lateral infiltration of seawater, which was very warm at this station. While none of the floes were flooded at the time of sampling, the top of the Mertz3 core (collected near the center of the floe) was highly porous and wet. The observed bulk salinity peak at 0.25–0.35 m was either the result of recent surface flooding or lateral infiltration through high-porosity layers near the top of the sea ice (Figure 5b). While percolation thresholds are probably higher in granular ice due to brine having to take a more convoluted path around ice

crystals, lateral percolation, and eventually dissociation of ice crystals, should be easier with brine inclusions between granular grains compared to the parallel layers of brine within the vertical columnar grains (Eicken & Lange, 1989).

The high-porosity layer near the top of Mertz3 was likely formed by either internal melting or a freezing front traveling through slush capped by a layer of superimposed or snow ice (Ackley et al., 2008; Fritsen et al., 1998; Haas et al., 2001). The measured brine salinity and $Si(OH)_4$ concentration matching the underlying seawater values support this hypothesis. Sea-ice NO_x in the high-porosity layer was likely depleted relative to underlying seawater values by a non-siliceous inoculum community possibly dominated by flagellates such as *Phaeocystis* spp. (e.g., Carnat et al., 2016; Tison et al., 2010; van Leeuwe et al., 2018). Phaeopigment to total chlorophyll pigment ratios of this community were high (28.4%; Figure 7) relative to other chl *a* peaks found during this study, and considerably higher than in the low light interior of sea ice in the Ross and Amundsen seas in summer when the algal bloom was starting and the chl *a* pool had not been degraded yet (3.8% from Arrigo et al., 2014). This suggests that either grazers were producing phaeopigments through sloppy feeding (Arrigo et al., 1991), or that the community was simply relatively old and degraded. If the latter, the accumulation of phaeopigments suggests that degradation products could not be exported out of this system, possibly due to brine stratification and entrapment in the ice matrix (Krembs et al., 2011). Phosphate and NH_3 were also accumulated, to higher concentrations than theoretical winter stocks (Table S3 in Supporting Information S1), indicating remineralization and/or grazing and subsequent adsorption within the sea ice (Fripiat et al., 2017).

4.2. Internal High-Porosity Layers Formed by Granular Decay and Rafting

There were other internal algal assemblages, lower in the sea ice, present at most of the pack ice floes, except for at Mertz1 and Mertz2 which were characterized by low concentration bottom algal assemblages (Figure 7). At Totten1 there was an internal algal assemblage, but no gap observed nor was rafting likely as the floe was large and level. Unfortunately, the texture core was not long enough to capture the ice around the algal assemblage. However, it is possible that the algae were in a high-porosity granular ice layer due to the presence of platelet ice which is associated with deep glacial-melt input, which can also supply frazil ice and associated organic matter and nutrients. An alternative explanation for the incorporated platelet ice found in this study is surface melt, which we think would have included a high proportion of snowmelt (see Section 4.1.1), percolating through the ice column to form under-ice melt ponds which grow ice platelets (Eicken, 1994; Martin & Kauffman, 1974; Tang et al., 2007). However, glacial-melt input appears more likely due to the proximity of ice stations to ice shelves, and in the case of Totten1, known ISW outflow (Moreau et al., 2019; Silvano et al., 2017).

SR3-5 was far from glacial-sources but also had a deep high-porosity layer harboring an algal community (Figures 7 and 8b). Positive $\delta^{18}O$ values below 0.1 m suggests that this floe topped with meteoric ice was not under-rafted. Granular layers can grow with frazil input by leads. Frazil formed in leads can descend with brine plumes and be advected under an ice cover or winds can push floes over the buoyantly ascending ice crystals (Weeks & Ackley, 1982). To continue thermodynamic growth below the granular layer, without negative oceanic heat flux from a source like ISW, the granular layer would have had to have been consolidated. This makes it unlikely that the gap was formed by partial refreezing of granular crystals, which is a mechanism for forming gap layers at the top of sea ice (Fritsen et al., 1998). Instead, the granular layer would have had to decay. The decay might have been accelerated by seawater, advected in from floe edges, boring out the pores of the granular layer (Haas et al., 2001).

Ice around the deep seawater-filled gap hosting an internal algal assemblage at Casey3 had a negative $\delta^{18}O$ peak and the floe appeared rafted from field observations. However, according to $\delta^{18}O$, there was a very high snow contribution at the top. An alternative explanation for the gap is that it formed as a gap layer at the top before considerable snow-loading and surface flooding formed a very thick layer of snow ice. Totten2's internal assemblage also coincided with a negative $\delta^{18}O$ peak and was probably decayed snow ice on top of an under-rafted floe, which agrees with field observations of two rafted floes.

The deep high-porosity layers helped to describe our macro-nutrient depth profiles, which were similar in shape to those described by Fripiat et al. (2017) for West Antarctic summer pack ice. The deep high-porosity layers also helped to explain our chl *a* depth profiles with peaks present in some, but not all, of the layers. These internal assemblages dominated the sampled chl *a* pool, in contrast to the study of Meiners et al. (2012) who showed

a 1:1.6 internal to surface assemblage ratio for integrated chl *a* in the Pacific Sector. This difference is likely the result of a general under-representation of Pacific Sector and summer data in the ASPeCt—Bio database (Meiners et al., 2012). We note that pack ice floes with incorporated layers of granular crystals due to glacial-melt input, rafting and very thick snow ice have previously been undersampled, especially at times when these layers have likely decayed to the point of allowing lateral infiltration of seawater and sustaining internal assemblages.

4.3. Floe Origins and Fates

4.3.1. Pack Ice Floes Incorporated Into Fast Ice

Casey3, Totten2 and SR3-5 were sampled relatively far from the coast and had long drift tracks that went forward to terminate at the fast ice edge. Interestingly, Casey3 and Totten2's back trajectories originated at the 1 Nov 2016 ice edge (Figure 3) suggesting that they retreated with the ice edge in spring. Convergence was strongest for the Casey3 back trajectory (Figure S8 in Supporting Information S1) and it likely explains why this floe was so thick (6.5 m as observed from the ship). As it is unlikely that these floes formed at the ice edge north of 64°S in late spring, we suspect that they were advected out there during the previous autumn/winter's sea-ice advance. This presents a process whereby sea ice might have moved offshore to where it was more prone to dynamic thickening (Eicken & Lange, 1989), before returning to the coast and possibly being incorporated in persistent fast ice. Ice edge compaction events that solidify pack ice in place have been described around the West Antarctic Peninsula (Massom et al., 2008). If incorporated, Casey3 and Totten2 might have introduced thicker ice to the fast ice. All the pack ice floes terminating in the fast ice might have introduced both surface and deep high-porosity layers with internal algal assemblages not normally associated with fast ice (e.g., Casey1 from O'Brien Bay). This could increase the productivity of these persistently ice-covered areas, at least at the periphery where floes such as these could be incorporated.

4.3.2. Floes With Glacial-Melt Input That Melted in Summer

By the end of January, Mertz1 had melted at the western ice edge of the Mertz Polynya and Mertz2 had melted at the calving face of the Mertz Glacier (Figure S9 in Supporting Information S1). While they did not house significant internal algal assemblages, these floes, along with the lower section of Mertz3, did have what appeared to be deep high-porosity layers. Numerous thin layers of granular ice at Mertz1, two of which already housed breaks, and platelet ice (Figure S3 in Supporting Information S1) indicated glacial-melt input. Intermittent inputs in Mertz1 could be explained by its drifting along the coast past several glacial-melt sources. Mertz1 was within 80 km from the coast for 20.5% of its back trajectory (Figure 3) and ice platelet crystals have previously been found at least 80 km from ice shelves (P. J. Langhorne, personal communication, 2019). Mertz2 originating and persisting near grounded icebergs and the Mertz and Ninnis glaciers (Figure S9 in Supporting Information S1) along with extensive negative $\delta^{18}O$ granular ice supports sustained glacial-melt input. However, if the platelet-like texture present at 1.14–1.30 m was instead old under-rafted columnar ice, most of the overlying ice was likely snow ice because rafting is generally constrained to ice thicknesses up to about 0.3 m (i.e., snow ice on top of two rafted floes from 0.7 to 1.3 m; Eicken & Lange, 1989). Either explanation introduces granular ice.

As described in Section 4.2, granular textures may be particularly susceptible to becoming high-porosity layers which may explain the short projected lifetimes of the floes that contained them. Salinity-normalized $Si(OH)_4$ values at the top of Mertz1 and Mertz2 were close to theoretical winter values (Figure 6c). Otherwise, macro-nutrient concentrations were low relative to Totten1 where we suggested platelet ice may have incorporated algal communities that retain macro-nutrients, and Mertz3 where there was some macro-nutrient enrichment from seawater infiltration (Figure 6). There were subtle differences in trajectories that might explain why macro-nutrient concentrations at Mertz1 and Mertz2 were different to nearby stations: Mertz1 passed further from the iceberg and fast ice conglomerate than SR3-5, and Mertz3 drifted south toward the coast initially while Mertz2 drifted west into the Mertz Polynya. In the process of melting, Mertz1 and Mertz2 floes would have diluted the already low surface water concentrations of NO_x, $Si(OH)_4$ and PO_4^{3-} and had little effect on NH_3.

4.4. Comparison With Spring Sea Ice From Conceptual Model

Figure 1 shows that spring sea-ice properties are described by Cold stage 1 (Zhou et al., 2013) and Transition stage a (Tison et al., 2008; Zhou et al., 2013). During Cold stage 1, there is a strong temperature gradient in the

ice. The top of the ice is very cold, and the brine density profile is unstable, but maintained by low permeability in most of the ice column. Brine convection is active in bottom ice. During Transition stage a, the temperature profile moves toward isothermal. Permeability increases above the bottom ice and brine convection can occur over the full-ice-depth, increasing access to and introducing nutrient-laden seawater to the ice interior. The timing of Transition stage a aligns with peak sea-ice primary production (Arrigo, 2017). If Transition stage a and summer stages were to occur earlier with future warming, the timing and magnitude of peak sea-ice primary production may be affected by changes in the habitable space between spring and summer stages, for example, the development of deep high-porosity layers.

4.5. Possible Future Impacts on Biogeochemical Processes

In the Arctic, atmospheric warming may lead to spring-summer sea ice becoming warmer and more permeable. This is expected to increase primary productivity and heterotrophy in the ice, but also to shift the system toward smaller algae and zooplankton that retain material within the sea ice rather than export it (Lannuzel et al., 2020). A retention system may be more optimal for sea-ice communities when brine is stratified, which should occur earlier with percolation thresholds being reached earlier in the season due to warmer ice. Antarctic fast ice is also expected to reach percolation thresholds earlier in the season in the future, with model projections showing warmer near-surface air temperatures and thinner ice (Fraser et al., 2022, Preprint). However, the insulating properties of Antarctica's spring snowpack would be bolstered by projected snowfall increases while at the same time being hindered by projected rainfall increases, leading to uncertainties around permeability (Fraser et al., 2022, Preprint). In the Arctic, melt ponds may become more common in spring sea ice in the future (Lannuzel et al., 2020). Melt ponds can be associated with dense algal colonies in the Arctic (Fernández-Méndez et al., 2014), and may become an increasingly important habitat around Antarctica under future warming.

5. Conclusions

The melt ponds and deep high-porosity layers found during this study could increase the movement of material through rotten sea ice. Material movement would otherwise be limited to molecular diffusion through stratified brine, heavily influenced by snowmelt as found here, and limited by low permeability superimposed and interposed ice. In addition, internal algal assemblages, in deep high-porosity layers, were more common than previously found for this part of Antarctica. We attribute deep high-porosity layers to the decay of granular ice that has either been submerged by snow ice accumulation on top or grown by frazil incorporation at the bottom. Descriptions of melt ponds and deep high-porosity layers in Antarctic sea ice are few. As they may become increasingly common habitats under future warming, melt ponds and highly porous sea ice should be an important focus of future observational studies as well as considered in sea-ice physico-biogeochemical models.

Conflict of Interest

The authors declare no conflicts of interest relevant to this study.

Data Availability Statement

Data presented here is available via the Australian Antarctic Data Centre (https://doi.org/10.26179/1rqm-tw41).

References

Ackley, S. F., Lewis, M. J., Fritsen, C. H., & Xie, H. (2008). Internal melting in Antarctic sea ice: Development of "gap layers". *Geophysical Research Letters*, 35(11), L11503. https://doi.org/10.1029/2008GL033644

Ackley, S. F., & Sullivan, C. W. (1994). Physical controls on the development and characteristics of Antarctic sea ice biological communities—A review and synthesis. *Deep Sea Research Part I: Oceanographic Research Papers*, 41(10), 1583–1604. https://doi.org/10.1016/0967-0637(94)90062-0

Andreas, E. L., & Ackley, S. F. (1982). On the differences in ablation seasons of Arctic and Antarctic sea ice. *Journal of the Atmospheric Sciences*, 39(2), 440–447. https://doi.org/10.1175/1520-0469(1982)039<0440:OTDIAS>2.0.CO;2

Armstrong, F. A. J., Stearns, C. R., & Strickland, J. D. H. (1967). The measurement of upwelling and subsequent biological process by means of the Technicon Autoanalyzer® and associated equipment. *Deep-Sea Research and Oceanographic Abstracts*, 14(3), 381–389. https://doi.org/10.1016/0011-7471(67)90082-4

Arrigo, K. R. (2017). Sea ice as a habitat for primary producers. In D. N. Thomas (Ed.), *Sea ice* (3 ed., pp. 352–369). John Wiley & Sons Ltd.

Arrigo, K. R., Brown, Z. W., & Mills, M. M. (2014). Sea ice algal biomass and physiology in the Amundsen Sea, Antarctica. *Elementa: Science of the Anthropocene*, *2*. https://doi.org/10.12952/journal.elementa.000028

Arrigo, K. R., Mock, T., & Lizotte, M. P. (2010). Primary producers and sea ice. In D. N. Thomas & G. S. Dieckmann (Eds.), *Sea ice* (2 ed., pp. 283–325). Blackwell Publishing Ltd.

Arrigo, K. R., Sullivan, C. W., & Kremer, J. N. (1991). A bio-optical model of Antarctic sea ice. *Journal of Geophysical Research*, *96*(C6), 10581–10592. https://doi.org/10.1029/91JC00455

Assur, A. (1958). Composition of sea ice and its tensile strength. Paper presented at the Arctic Sea Ice Conference.

Becquevort, S., Dumont, I., Tison, J.-L., Lannuzel, D., Sauvée, M.-L., Chou, L., & Schoemann, V. (2009). Biogeochemistry and microbial community composition in sea ice and underlying seawater off East Antarctica during early spring. *Polar Biology*, *32*(6), 879–895. https://doi.org/10.1007/s00300-009-0589-2

Bluhm, B. A., Gradinger, R. R., & Schnack-Schiel, S. B. (2010). Sea ice meio-and macrofauna. In D. N. Thomas & G. S. Dieckmann (Eds.), *Sea ice* (2 ed., pp. 357–393). Blackwell Publishing Ltd.

Carnat, G., Brabant, F., Dumont, I., Vancoppenolle, M., Ackley, S., Fritsen, C., et al. (2016). Influence of short-term synoptic events and snow depth on DMS, DMSP, and DMSO dynamics in Antarctic spring sea ice. *Elementa: Science of the Anthropocene*, *4*. https://doi.org/10.12952/journal.elementa.000135

Caron, D. A., Gast, R. J., & Garneau, M.-È. (2017). Sea ice as a habitat for micrograzers. In D. N. Thomas (Ed.), *Sea ice* (3 ed., pp. 370–393). John Wiley & Sons Ltd.

Cox, G. F. N., & Weeks, W. F. (1983). Equations for determining the gas and brine volumes in sea-ice samples. *Journal of Glaciology*, *29*(102), 306–316. https://doi.org/10.1017/s0022143000008364

Dempsey, D. E., & Langhorne, P. J. (2012). Geometric properties of platelet ice crystals. *Cold Regions Science and Technology*, *78*, 1–13. https://doi.org/10.1016/j.coldregions.2012.03.002

Dieckmann, G. S., & Hellmer, H. H. (2010). The importance of sea ice: An overview. In D. N. Thomas & G. S. Dieckmann (Eds.), *Sea ice* (2 ed., pp. 1–22). Blackwell Publishing Ltd.

Dieckmann, G. S., Rohardt, G., Hellmer, H., & Kipfstuhl, J. (1986). The occurrence of ice platelets at 250 m depth near the Filchner Ice Shelf and its significance for sea ice biology. *Deep-Sea Research, Part A: Oceanographic Research Papers*, *33*(2), 141–148. https://doi.org/10.1016/0198-0149(86)90114-7

Eicken, H. (1994). Structure of under-ice melt ponds in the central Arctic and their effect on, the sea-ice cover. *Limnology & Oceanography*, *39*(3), 682–693. https://doi.org/10.4319/lo.1994.39.3.0682

Eicken, H. (1998). Deriving modes and rates of ice growth in the Weddell Sea from microstructural, salinity and stable-isotope data. In M. O. Jeffries (Ed.), *Antarctic sea ice: Physical processes, interactions and variability* (Vol. 74, pp. 89–122). American Geophysical Union.

Eicken, H., & Lange, M. A. (1989). Development and properties of sea ice in the coastal regime of the southeastern Weddell Sea. *Journal of Geophysical Research*, *94*(C6), 8193–8206. https://doi.org/10.1029/JC094iC06p08193

Feltham, D. L., Untersteiner, N., Wettlaufer, J. S., & Worster, M. G. (2006). Sea ice is a mushy layer. *Geophysical Research Letters*, *33*(14), L14501. https://doi.org/10.1029/2006GL026290

Fernández-Méndez, M., Wenzhöfer, F., Peeken, I., Sørensen, H. L., Glud, R. N., & Boetius, A. (2014). Composition, buoyancy regulation and fate of ice algal aggregates in the central Arctic Ocean. *PLoS One*, *9*(9), e107452. https://doi.org/10.1371/journal.pone.0107452

Frantz, C. M., Light, B., Farley, S. M., Carpenter, S., Lieblappen, R., Courville, Z., et al. (2019). Physical and optical characteristics of heavily melted "rotten" Arctic sea ice. *The Cryosphere*, *13*(3), 775–793. https://doi.org/10.5194/tc-13-775-2019

Fraser, A. D., Massom, R. A., Michael, K. J., Galton-Fenzi, B. K., & Lieser, J. L. (2012). East Antarctic landfast sea ice distribution and variability, 2000–08. *Journal of Climate*, *25*(4), 1137–1156. https://doi.org/10.1175/JCLI-D-10-05032.1

Fraser, A. D., Massom, R. A., Ohshima, K. I., Willmes, S., Kappes, P. J., Cartwright, J., & Porter-Smith, R. (2020). High-resolution mapping of circum-Antarctic landfast sea ice distribution, 2000–2018. *Earth System Science Data*, *12*(4), 2987–2999. https://doi.org/10.5194/essd-12-2987-2020

Fraser, A. D., Wongpan, P., Langhorne, P. J., Klekociuk, A. R., Kusahara, K., Lannuzel, D., et al. (2022). Antarctic landfast sea ice: Physical, biogeochemical and ecological significance. *Earth and Space Science Open Archive*, *100*. https://doi.org/10.1002/essoar.10512682.1

Fripiat, F., Meiners, K. M., Vancoppenolle, M., Papadimitriou, S., Thomas, D. N., Ackley, S. F., et al. (2017). Macro-nutrient concentrations in Antarctic pack ice: Overall patterns and overlooked processes. *Elementa: Science of the Anthropocene*, *5*, 13. https://doi.org/10.1525/elementa.217

Fritsen, C. H., Ackley, S. F., Kremer, J. N., & Sullivan, C. W. (1998). Flood-freeze cycles and microalgal dynamics in Antarctic pack ice. *Antarctic sea ice: biological processes, interactions and variability*, *73*, 1–21. https://doi.org/10.1029/AR073p0001

Fritsen, C. H., Lytle, V. I., Ackley, S. F., & Sullivan, C. W. (1994). Autumn bloom of Antarctic pack-ice algae. *Science*, *266*(5186), 782–784. https://doi.org/10.1126/science.266.5186.782

Galindo, V., Levasseur, M., Mundy, C. J., Gosselin, M., Tremblay, J. É., Scarratt, M., et al. (2014). Biological and physical processes influencing sea ice, under-ice algae, and dimethylsulfoniopropionate during spring in the Canadian Arctic Archipelago. *Journal of Geophysical Research: Oceans*, *119*(6), 3746–3766. https://doi.org/10.1002/2013JC009497

Golden, K. M., Ackley, S. F., & Lytle, V. I. (1998). The percolation phase transition in sea ice. *Science*, *282*(5397), 2238–2241. https://doi.org/10.1126/science.282.5397.2238

Greene, C. A., Gwyther, D. E., & Blankenship, D. D. (2017). Antarctic mapping tools for MATLAB. *Computers & Geosciences*, *104*, 151–157. https://doi.org/10.1016/j.cageo.2016.08.003

Günther, S., & Dieckmann, G. S. (1999). Seasonal development of algal biomass in snow-covered fast ice and the underlying platelet layer in the Weddell Sea, Antarctica. *Antarctic Science*, *11*(3), 305–315. https://doi.org/10.1017/S0954102099000395

Haas, C., Thomas, D. N., & Bareiss, J. (2001). Surface properties and processes of perennial Antarctic sea ice in summer. *Journal of Glaciology*, *47*(159), 613–625. https://doi.org/10.3189/172756501781831864

Hegseth, E. N., & Von Quillfeldt, C. H. (2002). Low phytoplankton biomass and ice algal blooms in the Weddell Sea during the ice-filled summer of 1997. *Antarctic Science*, *14*(3), 231–243. https://doi.org/10.1017/S095410200200007X

Holm-Hansen, O., Lorenzen, C. J., Holmes, R. W., & Strickland, J. D. H. (1965). Fluorometric determination of chlorophyll. *ICES Journal of Marine Science*, *30*(1), 3–15. https://doi.org/10.1093/icesjms/30.1.3

Hoppmann, M., Richter, M. E., Smith, I. J., Jendersie, S., Langhorne, P. J., Thomas, D. N., & Dieckmann, G. S. (2020). Platelet ice, the Southern Ocean's hidden ice: A review. *Annals of Glaciology*, *61*(83), 341–368. https://doi.org/10.1017/aog.2020.54

Hudier, E. J. J., Ingram, R. G., & Shirasawa, K. (1995). Upward flushing of sea water through first year ice. *Atmosphere-Ocean*, *33*(3), 569–580. https://doi.org/10.1080/07055900.1995.9649545

Jacobs, S. S., Fairbanks, R. G., & Horibe, Y. (1985). Origin and evolution of water masses near the Antarctic continental margin: Evidence from $H_2^{18}O/H_2^{16}O$ ratios in seawater. In S. S. Jacobs (Ed.), *Oceanology of the Antarctic continental shelf* (Vol. 43, pp. 59–85). American Geophysical Union.

Jardon, F. P., Vivier, F., Vancoppenolle, M., Lourenço, A., Bouruet-Aubertot, P., & Cuypers, Y. (2013). Full-depth desalination of warm sea ice. *Journal of Geophysical Research: Oceans*, *118*(1), 435–447. https://doi.org/10.1029/2012JC007962

Jeffries, M. O., Weeks, W. F., Shaw, R., & Morris, K. (1993). Structural characteristics of congelation and platelet ice and their role in the development of Antarctic land-fast sea ice. *Journal of Glaciology*, *39*(132), 223–238. https://doi.org/10.3189/S0022143000015884

Jordan, J. R., Kimura, S., Holland, P. R., Jenkins, A., & Piggott, M. D. (2015). On the conditional frazil ice instability in seawater. *Journal of Physical Oceanography*, *45*(4), 1121–1138. https://doi.org/10.1175/JPO-D-14-0159.1

Juhl, A. R., Krembs, C., & Meiners, K. M. (2011). Seasonal development and differential retention of ice algae and other organic fractions in first-year Arctic sea ice. *Marine Ecology Progress Series*, *436*, 1–16. https://doi.org/10.3354/meps09277

Kawamura, T., Jeffries, M. O., Tison, J.-L., & Krouse, H. R. (2004). Superimposed-ice formation in summer on Ross Sea pack-ice floes. *Annals of Glaciology*, *39*, 563–568. https://doi.org/10.3189/172756404781814168

Kérouel, R., & Aminot, A. (1997). Fluorometric determination of ammonia in sea and estuarine waters by direct segmented flow analysis. *Marine Chemistry*, *57*(3–4), 265–275. https://doi.org/10.1016/S0304-4203(97)00040-6

Kimura, N. (2004). Sea ice motion in response to surface wind and ocean current in the Southern Ocean. *Journal of the Meteorological Society of Japan. Series II*, *82*(4), 1223–1231. https://doi.org/10.2151/jmsj.2004.1223

Krembs, C., Eicken, H., & Deming, J. W. (2011). Exopolymer alteration of physical properties of sea ice and implications for ice habitability and biogeochemistry in a warmer Arctic. *Proceedings of the National Academy of Sciences*, *108*(9), 3653–3658. https://doi.org/10.1073/pnas.1100701108

Krinner, G., Magand, O., Simmonds, I., Genthon, C., & Dufresne, J.-L. (2007). Simulated Antarctic precipitation and surface mass balance at the end of the twentieth and twenty-first centuries. *Climate Dynamics*, *28*(2–3), 215–230. https://doi.org/10.1007/s00382-006-0177-x

Lange, M. A., Ackley, S. F., Wadhams, P., Dieckmann, G. S., & Eicken, H. (1989). Development of sea ice in the Weddell Sea. *Annals of Glaciology*, *12*, 92–96. https://doi.org/10.3189/S0260305500007023

Langhorne, P. J., Hughes, K. G., Gough, A. J., Smith, I. J., Williams, M. J. M., Robinson, N. J., et al. (2015). Observed platelet ice distributions in Antarctic sea ice: An index for ocean-ice shelf heat flux. *Geophysical Research Letters*, *42*(13), 5442–5451. https://doi.org/10.1002/2015GL064508

Langway, C. C., Jr. (1958). *Ice fabrics and the universal stage*. Department of Defense, Department of the Army, Corps of Engineers. Snow Ice and Permafrost Research Establishment.

Lannuzel, D., Schoemann, V., de Jong, J., Tison, J.-L., & Chou, L. (2007). Distribution and biogeochemical behaviour of iron in the East Antarctic sea ice. *Marine Chemistry*, *106*(1–2), 18–32. https://doi.org/10.1016/j.marchem.2006.06.010

Lannuzel, D., Tedesco, L., van Leeuwe, M., Campbell, K., Flores, H., Delille, B., et al. (2020). The future of Arctic sea-ice biogeochemistry and ice-associated ecosystems. *Nature Climate Change*, *10*(11), 983–992. https://doi.org/10.1038/s41558-020-00940-4

Lewis, M. J., Tison, J.-L., Weissling, B. P., Delille, B., Ackley, S. F., Brabant, F., & Xie, H. (2011). Sea ice and snow cover characteristics during the winter–spring transition in the Bellingshausen Sea: An overview of SIMBA 2007. *Deep Sea Research Part II: Topical Studies in Oceanography*, *58*(9–10), 1019–1038. https://doi.org/10.1016/j.dsr2.2010.10.027

Light, B., Maykut, G. A., & Grenfell, T. C. (2003). Effects of temperature on the microstructure of first-year Arctic sea ice. *Journal of Geophysical Research*, *108*(C2). https://doi.org/10.1029/2001JC000887

Lorenzen, C. J. (1966). A method for the continuous measurement of in vivo chlorophyll concentration. *Deep-Sea Research and Oceanographic Abstracts*, *13*(2), 223–227. https://doi.org/10.1016/0011-7471(66)91102-8

Lytle, V. I., & Ackley, S. F. (1996). Heat flux through sea ice in the Western Weddell Sea: Convective and conductive transfer processes. *Journal of Geophysical Research*, *101*(C4), 8853–8868. https://doi.org/10.1029/95JC03675

Mahoney, A. R., Gough, A. J., Langhorne, P. J., Robinson, N. J., Stevens, C. L., Williams, M. M. J., & Haskell, T. G. (2011). The seasonal appearance of ice shelf water in coastal Antarctica and its effect on sea ice growth. *Journal of Geophysical Research*, *116*(C11). https://doi.org/10.1029/2011JC007060

Martin, S., & Kauffman, P. (1974). The evolution of under-ice melt ponds, or double diffusion at the freezing point. *Journal of Fluid Mechanics*, *64*(3), 507–528. https://doi.org/10.1017/S0022112074002527

Massom, R. A., Eicken, H., Hass, C., Jeffries, M. O., Drinkwater, M. R., Sturm, M., et al. (2001). Snow on Antarctic sea ice. *Reviews of Geophysics*, *39*(3), 413–445. https://doi.org/10.1029/2000RG000085

Massom, R. A., Stammerjohn, S. E., Lefebvre, W., Harangozo, S. A., Adams, N., Scambos, T. A., et al. (2008). West Antarctic Peninsula sea ice in 2005: Extreme ice compaction and ice edge retreat due to strong anomaly with respect to climate. *Journal of Geophysical Research*, *113*(C2), C02S20. https://doi.org/10.1029/2007JC004239

Meier, W. N., Fetterer, F., Windnagel, A. K., & Stewart, J. S. (2021). NOAA/NSIDC climate data record of passive microwave sea ice concentration, version 4. https://doi.org/10.7265/efmz-2t65

Meiners, K. M., Vancoppenolle, M., Carnat, G., Castellani, G., Delille, B., Delille, D., et al. (2018). Chlorophyll-a in Antarctic landfast sea ice: A first synthesis of historical ice core data. *Journal of Geophysical Research: Oceans*, *123*(11), 8444–8459. https://doi.org/10.1029/2018JC014245

Meiners, K. M., & Michel, C. (2017). Dynamics of nutrients, dissolved organic matter and exopolymers in sea ice. In D. N. Thomas (Ed.), *Sea ice* (3 ed., pp. 415–432). John Wiley & Sons Ltd.

Meiners, K. M., Vancoppenolle, M., Thanassekos, S., Dieckmann, G. S., Thomas, D. N., Tison, J.-L., et al. (2012). Chlorophyll *a* in Antarctic sea ice from historical ice core data. *Geophysical Research Letters*, *39*(21). https://doi.org/10.1029/2012gl053478

Miller, L. A., Fripiat, F., Else, B. G. T., Bowman, J. S., Brown, K. A., Collins, R. E., et al. (2015). Methods for biogeochemical studies of sea ice: The state of the art, caveats, and recommendations. *Elementa: Science of the Anthropocene*, *3*. https://doi.org/10.12952/journal.elementa.000038

Moreau, S., Lannuzel, D., Janssens, J. P. J., Arroyo, M. C., Corkill, M., Cougnon, E., et al. (2019). Sea ice meltwater and circumpolar deep water drive contrasting productivity in three Antarctic polynyas. *Journal of Geophysical Research: Oceans*, *124*(5), 2943–2968. https://doi.org/10.1029/2019jc015071

Morris, K., & Jeffries, M. O. (2001). Seasonal contrasts in snow-cover characteristics on Ross Sea ice floes. *Annals of Glaciology*, *33*, 61–68. https://doi.org/10.3189/172756401781818608

Mouginot, J., Scheuchl, B., & Rignot, E. (2017). MEaSUREs Antarctic boundaries for IPY 2007-2009 from satellite radar, version 2.

Murphy, J., & Riley, J. P. (1962). A modified single solution method for the determination of phosphate in natural waters. *Analytica Chimica Acta*, *27*, 31–36. https://doi.org/10.1016/S0003-2670(00)88444-5

Nomura, D., Yoshikawa-Inoue, H., Toyota, T., & Shirasawa, K. (2010). Effects of snow, snowmelting and refreezing processes on air–sea-ice C_O2 flux. *Journal of Glaciology*, *56*(196), 262–270. https://doi.org/10.3189/002214310791968548

Parkinson, C. L. (2019). A 40-y record reveals gradual Antarctic sea ice increases followed by decreases at rates far exceeding the rates seen in the Arctic. *Proceedings of the National Academy of Sciences*, *116*(29), 14414–14423. https://doi.org/10.1073/pnas.1906556116

Perovich, D. K., Roesler, C. S., & Pegau, W. S. (1998). Variability in Arctic sea ice optical properties. *Journal of Geophysical Research*, *103*(C1), 1193–1208. https://doi.org/10.1029/97JC01614

Petrich, C., & Eicken, H. (2010). Growth, structure and properties of sea ice. In D. N. Thomas & G. S. Dieckmann (Eds.), *Sea ice* (2 ed., pp. 23–77). Blackwell Publishing Ltd.

Polashenski, C., Perovich, D., & Courville, Z. (2012). The mechanisms of sea ice melt pond formation and evolution. *Journal of Geophysical Research*, *117*(C1). https://doi.org/10.1029/2011JC007231

Pounder, E. R. (1965). *The physics of ice*. In J. A. Jacobs & J. T. Wilson (Eds.), (1 ed.). Pergamon Press Ltd.

Rees, C., Pender, L., Sherrin, K., Schwanger, C., Hughes, P., Tibben, S., et al. (2019). Methods for reproducible shipboard SFA nutrient measurement using RMNS and automated data processing. *Limnology and Oceanography: Methods*, *17*(1), 25–41. https://doi.org/10.1002/lom3.10294

Rignot, E., Jacobs, S., Mouginot, J., & Scheuchl, B. (2013). Ice-shelf melting around Antarctica. *Science*, *341*(6143), 266–270. https://doi.org/10.1126/science.1235798

Silvano, A., Rintoul, S. R., Peña-Molino, B., & Williams, G. D. (2017). Distribution of water masses and meltwater on the continental shelf near the Totten and Moscow University ice shelves. *Journal of Geophysical Research: Oceans*, *122*(3), 2050–2068. https://doi.org/10.1002/2016JC012115

Spreen, G., Kaleschke, L., & Heygster, G. (2008). Sea ice remote sensing using AMSR-E 89-GHz channels. *Journal of Geophysical Research*, *113*(C2), C02S03. https://doi.org/10.1029/2005JC003384

Tang, S., Qin, D., Ren, J., Kang, J., & Li, Z. (2007). Structure, salinity and isotopic composition of multi-year landfast sea ice in Nella Fjord, Antarctica. *Cold Regions Science and Technology*, *49*(2), 170–177. https://doi.org/10.1016/j.coldregions.2007.03.005

Tian, T. R., Fraser, A. D., Kimura, N., Zhao, C., & Heil, P. (2022). Rectification and validation of a daily satellite-derived Antarctic sea ice velocity product. *The Cryosphere*, *16*(4), 1299–1314. https://doi.org/10.5194/tc-16-1299-2022

Timco, G. W., & Weeks, W. F. (2010). A review of the engineering properties of sea ice. *Cold Regions Science and Technology*, *60*(2), 107–129. https://doi.org/10.1016/j.coldregions.2009.10.003

Tison, J.-L., Brabant, F., Dumont, I., & Stefels, J. (2010). High-resolution dimethyl sulfide and dimethylsulfoniopropionate time series profiles in decaying summer first-year sea ice at Ice Station Polarstern, Western Weddell Sea, Antarctica. *Journal of Geophysical Research*, *115*(G4), G04044. https://doi.org/10.1029/2010JG001427

Tison, J.-L., Maksym, T., Fraser, A. D., Corkill, M., Kimura, N., Nosaka, Y., et al. (2020). Physical and biological properties of early winter Antarctic sea ice in the Ross Sea. *Annals of Glaciology*, *61*(83), 241–259. https://doi.org/10.1017/aog.2020.43

Tison, J.-L., Schwegmann, S., Dieckmann, G. S., Rintala, J.-M., Meyer, H., Moreau, S., et al. (2017). Biogeochemical impact of snow cover and cyclonic intrusions on the winter Weddell Sea ice pack. *Journal of Geophysical Research: Oceans*, *122*(12), 9548–9571. https://doi.org/10.1002/2017JC013288

Tison, J.-L., Worby, A. P., Delille, B., Brabant, F., Papadimitriou, S., Thomas, D. N., et al. (2008). Temporal evolution of decaying summer first-year sea ice in the Western Weddell Sea, Antarctica. *Deep Sea Research Part II: Topical Studies in Oceanography*, *55*(8–9), 975–987. https://doi.org/10.1016/j.dsr2.2007.12.021

Toyota, T., Smith, I. J., Gough, A. J., Langhorne, P. J., Leonard, G. H., Van Hale, R. J., et al. (2013). Oxygen isotope fractionation during the freezing of sea water. *Journal of Glaciology*, *59*(216), 697–710. https://doi.org/10.3189/2013JoG12J163

Vancoppenolle, M., Goosse, H., de Montety, A., Fichefet, T., Tremblay, B., & Tison, J.-L. (2010). Modeling brine and nutrient dynamics in Antarctic sea ice: The case of dissolved silica. *Journal of Geophysical Research*, *115*(C2), C02005. https://doi.org/10.1029/2009JC005369

Vancoppenolle, M., Madec, G., Thomas, M., & McDougall, T. J. (2019). Thermodynamics of sea ice phase composition revisited. *Journal of Geophysical Research: Oceans*, *124*(1), 615–634. https://doi.org/10.1029/2018JC014611

Vancoppenolle, M., Meiners, K. M., Michel, C., Bopp, L., Brabant, F., Carnat, G., et al. (2013a). Role of sea ice in global biogeochemical cycles: Emerging views and challenges. *Quaternary Science Reviews*, *79*, 207–230. https://doi.org/10.1016/j.quascirev.2013.04.011

Vancoppenolle, M., Notz, D., Vivier, F., Tison, J. L., Delille, B., Carnat, G., et al. (2013). On the use of the mushy-layer Rayleigh number for the interpretation of sea-ice-core data. *The Cryosphere Discussions*, *7*(4), 3209–3230. https://doi.org/10.5194/tcd-7-3209-2013

van Leeuwe, M. A., Tedesco, L., Arrigo, K. R., Assmy, P., Campbell, K., Meiners, K. M., et al. (2018). Microalgal community structure and primary production in Arctic and Antarctic sea ice: A synthesis. *Elementa: Science of the Anthropocene*, *6*. https://doi.org/10.1525/elementa.267

Wadhams, P., Lange, M. A., & Ackley, S. F. (1987). The ice thickness distribution across the Atlantic sector of the Antarctic Ocean in midwinter. *Journal of Geophysical Research*, *92*(C13), 14535–14552. https://doi.org/10.1029/JC092iC13p14535

Weeks, W. F., & Ackley, S. F. (1982). *The growth, structure, and properties of sea ice (CRREL monograph 82-1)*. Retrieved from US Army Corps of Engineers, Cold Regions Research & Engineering Laboratory. Retrieved from https://apps.dtic.mil/dtic/tr/fulltext/u2/a123762.pdf

Wells, A. J., Hitchen, J. R., & Parkinson, J. R. G. (2019). Mushy-layer growth and convection, with application to sea ice. *Philosophical Transactions of the Royal Society A*, *377*(2146), 20180165. https://doi.org/10.1098/rsta.2018.0165

Wongpan, P., Hughes, K. G., Langhorne, P. J., & Smith, I. J. (2018). Brine convection, temperature fluctuations, and permeability in winter Antarctic land-fast sea ice. *Journal of Geophysical Research: Oceans*, *123*(1), 216–230. https://doi.org/10.1002/2017JC012999

Wood, E. D., Armstrong, F. A. J., & Richards, F. A. (1967). Determination of nitrate in sea water by cadmium-copper reduction to nitrite. *Journal of the Marine Biological Association of the United Kingdom*, *47*(1), 23–31. https://doi.org/10.1017/S002531540003352X

Worby, A. P., Geiger, C. A., Paget, M. J., Van Woert, M. L., Ackley, S. F., & DeLiberty, T. L. (2008). Thickness distribution of Antarctic sea ice. *Journal of Geophysical Research*, *113*(C5), C05S92. https://doi.org/10.1029/2007JC004254

Worby, A. P., & Massom, R. A. (1995). *The structure and properties of sea ice and snow cover in East Antarctic pack ice (7)*. Retrieved from Antarctic Cooperative Research Centre Research

World Meteorological Organization. (2014). *Sea ice nomenclature*. Retrieved from https://library.wmo.int/doc_num.php?explnum_id=4651

Worster, M. G., & Rees Jones, D. W. (2015). Sea-ice thermodynamics and brine drainage. *Philosophical Transactions of the Royal Society A: Mathematical, Physical & Engineering Sciences*, *373*(2045), 20140166. https://doi.org/10.1098/rsta.2014.0166

Zhou, J., Delille, B., Eicken, H., Vancoppenolle, M., Brabant, F., Carnat, G., et al. (2013). Physical and biogeochemical properties in landfast sea ice (Barrow, Alaska): Insights on brine and gas dynamics across seasons. *Journal of Geophysical Research: Oceans*, *118*(6), 3172–3189. https://doi.org/10.1002/jgrc.20232

Zubov, N. N. (1945). *Arctic ice (Izdatel'stvo Glavsevmoputi)* (p. 217). US Naval Oceanographic Office Translation.